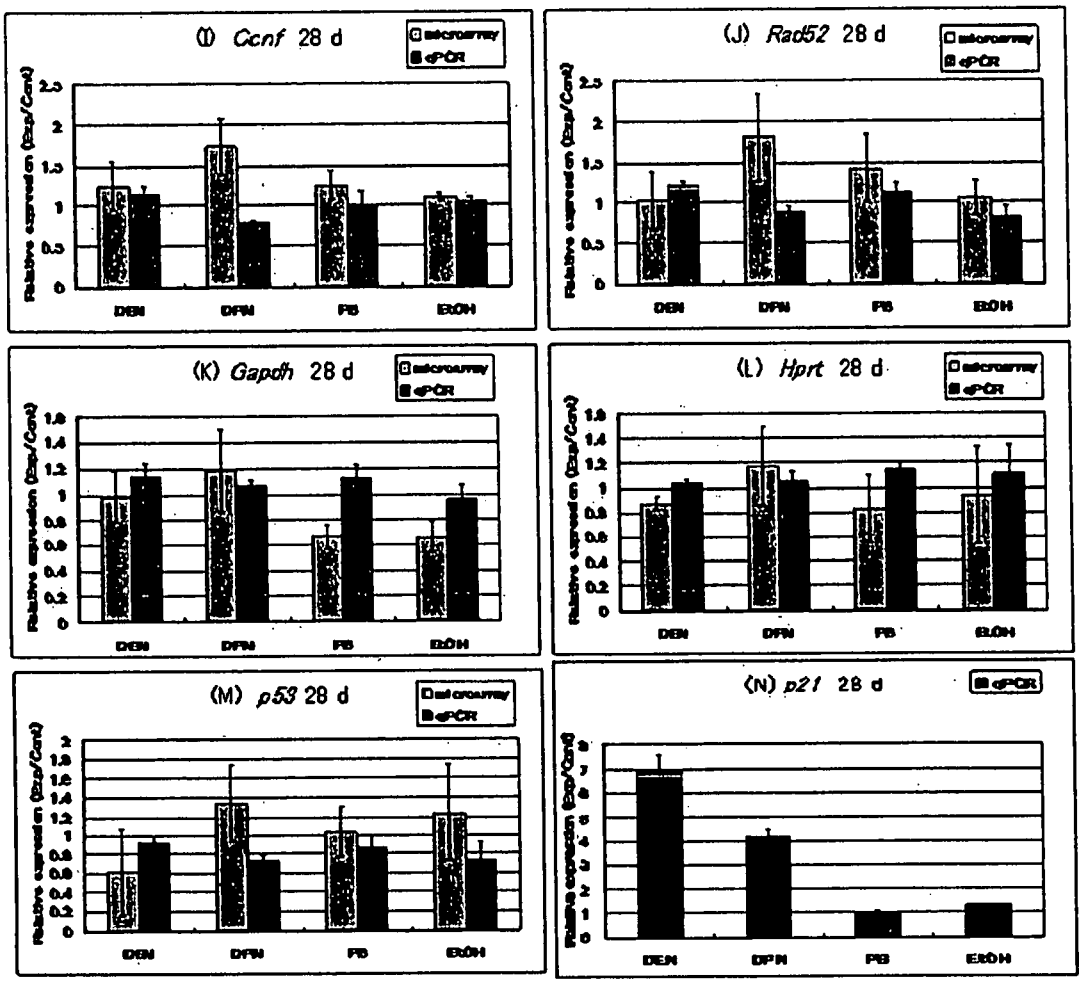

Fig. 4. Verification of DNA microarray results with qPCR 28 days after chemical administration (Experiment II). Results are shown as average and SD (error bar), and expressed as relative expression (experimental group/vehicle control group). Microarray: data are from 4 spots from two microarrays for DEN and DPN, and from 4 spots from one microarray for PB and EtOH. qPCR: results from triplicate assays. mRNA or total RNA from pooled livers from 5 mice was used as material. Only qPCR result is shown for *p21*.

not newly appear at 28 days after administration. PB and EtOH did not show significant increase or decrease of gene expression 28 days after administration. In conclusion, acute responses to the genotoxic carcinogens remained only partially in liver 28 days after administration, while PB and EtOH did not induce significant acute or longer term gene expression changes in the 268 gene-list.

Figs. 3 and 4 show that standard deviation in data sets was generally smaller in qPCR (3 tubes per experiment) than DNA microarray (4 spots per experiment). Fluorescence intensity was very similar in another experiment of the same gene (*Gapdh, Ccngl, c-Jun, Rad52, Hsp27* and others) in qPCR, indicating good reproducibility. However, fluorescence intensity in a repeat DNA microarray experiment was less reproducible, likely due to variability in fluorescent labeling of cDNA and washing of DNA microarray even if a similar amount of DNA is used for hybridization with the same lot of DNA microarray. The reliability and reproducibility of experiments are higher with qPCR than with DNA microarray in the present experimental conditions.

We demonstrated that inter-individual variation was small for all 5 genes assayed with qPCR and examined 4 h and 28 days after administration in 5 control and 5 DEN-treated mice (Fig. 5). These individual results matched well the qPCR results in Fig. 3 and Fig. 4, where liver samples of 5 different mice were pooled and assayed. Based on this, we mainly conducted experiments using pooled liver samples of 5 mice (Experiment II), although experiments using individual animal

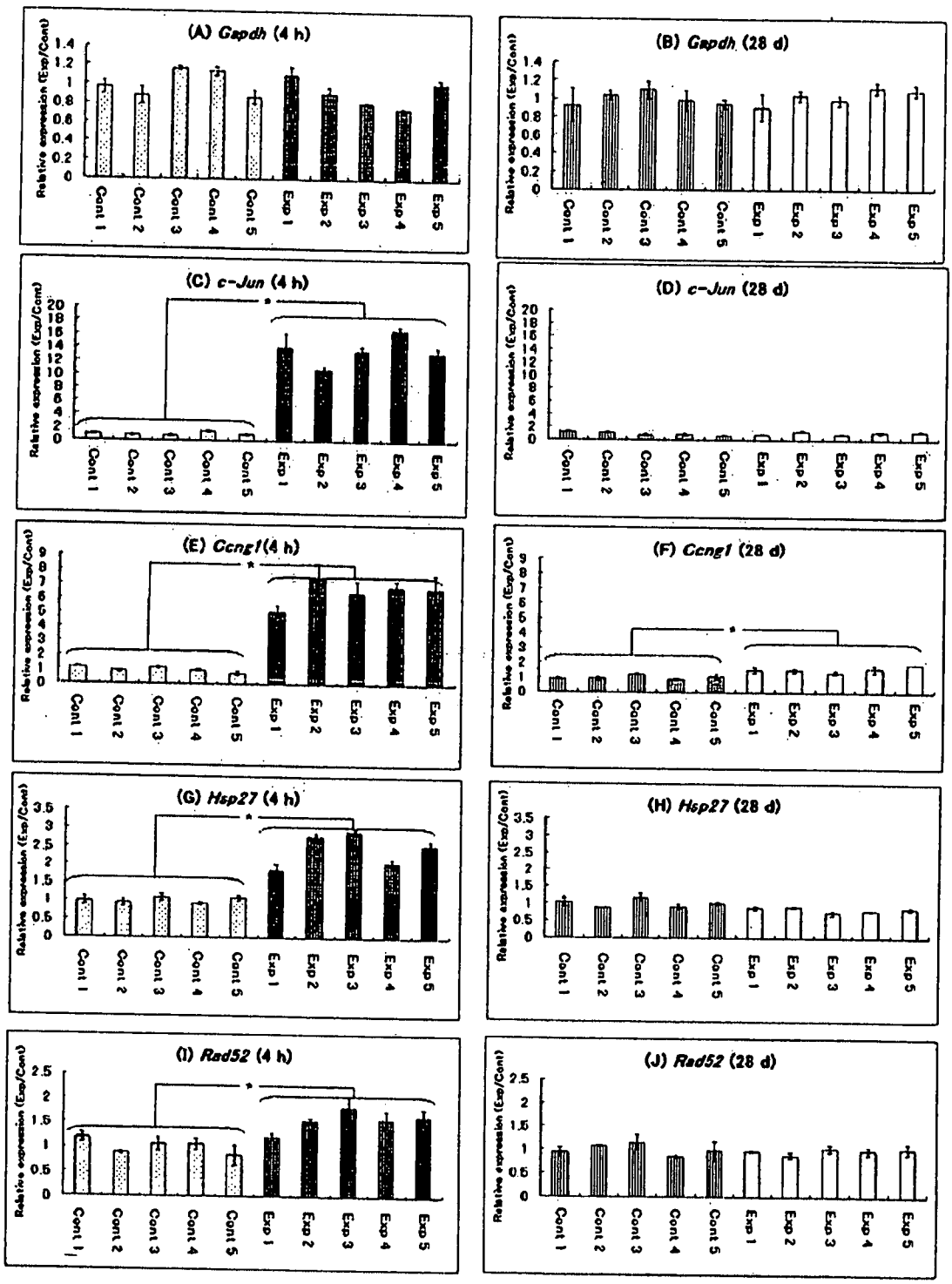

Fig. 5. Variation among individual mice (relative liver gene expression) (Experiment III). DEN (80 mg/kg bw) and saline were given to 9-week-old mice (5 per group), main lobe of liver was dissected individually after 4 h and 28 days and individual gene expression was determined with qPCR. cDNA from individual liver from 5 mice for each group was used as material. Gene expression of *Ccngl*, *c-Jun*, *Rad52* and *Hsp27* was normalized with gene expression of *Gapdh*. Values in *c-Jun* (4 h), *Ccngl* (4 h and 28 d), *Hsp27* (4 h) and *Rad53* (4 h) in DEN group were significantly different ($p < 0.01$) from control group.

Table 2. Variation among individuals determined with qPCR*

Group	Relative expression (Exp/Cont, Mean ± SD)				
	Gapdh	*c-Jun*	*Ccng1*	*Hsp27*	*Rad52*
Saline 4 h	1.00±0.14	1.00±0.26	1.00±0.18	1.00±0.07	1.00±0.14
DEN 4 h	0.92±0.14	13.71±2.11	6.50±0.86	2.47±0.47	1.56±0.23
Saline 28 d	1.00±0.07	1.00±0.24	1.00±0.16	1.00±0.12	1.00±0.12
DEN 28 d	1.03±0.09	1.15±0.26	1.57±0.21	0.83±0.07	0.97±0.06

*Experiment III, livers from 5 mice each of experimental groups (4 h and 28 days) and control group were used. Mean of control group is presented as 1.00.

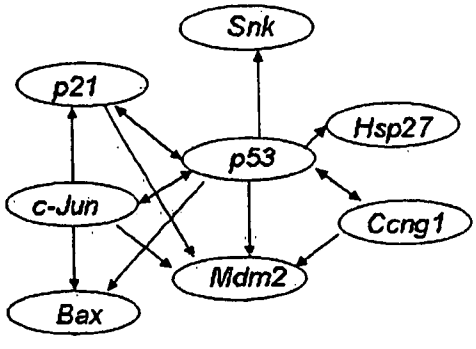

Fig. 6. Suggested gene network of seven *p53* target genes analyzed using Ingenuity Pathways Analysis.

material were desirable.

Recent reports have described changes in gene expression in DEN-induced mouse liver tumors (22–24) and DEN-treated rat liver (25) with different DNA microarrays containing different genes, but no studies have focused on the DNA damaging time of 4 h nor the mutation fixing time of 28 days; thus, different gene expressions were detected. As well, there are no reports which compare changes in gene expression in mouse liver for DEN and DPN exposures. The present study showed that DEN and DPN induced very similar changes in gene expression in mouse liver at 4 h and 28 days after their administration, suggesting a similar response mechanism. Gene expression changes with PB (25–27) and EtOH (28) were previously studied in mouse or rat liver at different time points with different DNA microarrays containing different genes, resulting in different gene expressions being detected.

In the present DNA microarray we mainly selected genes that have been linked with the action of genotoxic carcinogens. As a result we could find characteristic gene expression increases for DEN and DPN, but we could not find genes that were specifically responsive to the non-genotoxic carcinogen PB or to the non-carcinogenic toxin EtOH. Decreased-expression genes were observed among the 268 genes in the present results (not shown). However, characteristically decreased genes were not found for DEN, DPN, PB or EtOH in the present 268 gene-list.

In the first step of characterizing our microarray system, we examined 20mer, 30mer and 40–47mer oligonucleotides as probes (data not shown) and concluded that 40–47mer oligonucleotides showed sufficient strength of fluorescence. In an early trial, we prepared cDNA microarray with PCR products of 400 bp length. However these cDNA microarrays were less sensitive than the present oligonucleotide microarray (data not shown).

In conclusion, we have used DNA microarray and qPCR to show (1) that in comparison to PB and EtOH, the genotoxic carcinogens DEN and DPN induced differential gene expression in *p53* target genes in mouse liver 4 h after chemical administration (a time when DNA damage is induced by *N*-nitroso carcinogens), and (2) that these acute responses remained only partially in liver 28 days after administration, a time when little DNA damage remains but mutations are observed. We will continue further studies to add other useful genes to our DNA microarray, including high throughput DNA microarray studies in mouse liver and preparation of in-house oligonucleotide microarray for characterizing mutagenic and carcinogenic compounds; these data will be applied to the study of chemical risk assessment.

Acknowledgements: This work was partly supported by Special Coordination Funds for Promoting Science and Technology (C. Furihata and H. Tashiro) and by KAKENHI (18310047) (C. Furihata, T. Watanabe and T. Suzuki), The Ministry of Education, Culture, Sports, Science and Technology, Japan. We thank Drs. Yoshifumi Uno (Mitsubishi Pharma Co.), Yasuhito Yamamoto (Lion Co.), Yuko Saito (NIKKEN CHEMICALS CO., LTD), Kohji Yamakage (Hatano Research Institute, Food and Drug Safety Center) and Akihiro Wakata (Yamanouchi Pharmaceutical Co., Ltd.) (members of JEMS/MMS/Toxicogenomics collaborative study) for stimulating discussions.

References

1 Aardema MJ, MacGregor JT. Toxicology and genetic

toxicology in the new era of "toxicogenomics": impact of "-omics" technologies. Mutat Res. 2002; 499: 13-25.
2 Dupuy A, Simon RM. Critical review of published microarray studies for cancer outcome and guideline on statistical analysis and reporting. J Natl Cancer Inst. 2007; 99: 147-57.
3 Ulger C, Toruner GA, Alkan M, Mohammed M, Damani S, Kang J, Galante A, Aviv H, Soteropoulos P, Tolias PP, Schwalb MN, Dermody JJ. Comprehensive genome-wide comparison of DNA and RNA level scan using microarray technology for identification of candidate cancer-related genes in the HL-60 cell line. Cancer Genet Cytogenet. 2003; 147: 28-35.
4 Mecham BH, Klus GT, Strovel J, Augustus M, Byrne D, Bozso P, Wetmore GZ, Mariani TJ, Kohane IS, Szallasi S. Sequence-matched probes produce increased cross-platform consistency and more reproducible biological results in microarray-based gene expression measurements. Nucleic Acids Res. 2004; 32: e74.
5 Shippy R, Sendera TJ, Lockner R, Palaniappan C, Kaysser-Kranich T, Watts G, Alsobrook J. Performance evaluation of commercial short-oligonucleotide microarrays and the impact of noise in making cross-platform correlations. BMC Genomics. 2004; 5: 61.
6 Provenzano M, Mocellin S. Complementary techniques: validation of gene expression data by quantitative real time PCR. Adv Exp Med Biol. 2007; 593: 66-73.
7 Mientjes EJ, Luiten-Schuite A, van der Wolf E, Borsboom Y, Bergmans A, Berends F, Lohman PH, Baan RA, van Delft JH. DNA adducts, mutant frequencies, and mutation spectra in various organs of lambda lacZ mice exposed to ethylating agents. Environ Mol Mutagen. 1998; 31: 18-31.
8 Madle S, Dean SW, Andrae U, Brambilla G, Burlinson B, Doolittle DJ, Furihata C, Hertner T, McQueen CA, Mori H. Recommendations for the performance of UDS tests *in vitro* and *in vivo*. Mutat Res. 1994; 312: 263-85.
9 Sasaki YF, Sekihashi K, Izumiyama F, Nishidate E, Saga A, Ishida K, Tsuda S. The comet assay with multiple mouse organs: comparison of comet assay results and carcinogenicity with 208 chemicals selected from the IARC monographs and U.S. NTP Carcinogenicity Database. Crit Rev Toxicol. 2000; 30: 629-799.
10 Suzuki T, Hayashi M, Sofuni T. Initial experiences and future directions for transgenic mouse mutation assays. Mutat Res. 1994; 307: 489-94.
11 Suzuki T, Itoh S, Nakajima M, Hachiya N, Hara T. Target organ and time-course in the mutagenicity of five carcinogens in MutaMouse: a summary report of the second collaborative study of the transgenic mouse mutation assay by JEMS/MMS. Mutat Res. 1999; 444: 259-68.
12 Furihata C, Oka M, Yamamoto M, Ito T, Miki K, Tatematsu M, Sakaki Y, Reske K. Differentially expressed MHC class II-associated invariant chain in rat stomach pyloric mucosa with *N*-methyl-*N'*-nitro-*N*-nitrosoguanidine exposure, Cancer Res. 1997; 57: 1416-8.
13 Oka M, Furihata C, Kitoh K, Yamamoto M, Ichinose M, Miki K, Ito T, Sakaki Y, Reske K, Involvement of dendritic cell response to resistance of stomach carcinogenesis caused by *N*-methyl-*N'*-nitro-*N*-nitrosoguanidine in rats, Cancer Res. 1998; 58: 4107-12.
14 Strano S, Dell'orso S, Di Agostino S, Fontemaggi G, Sacchi A, Blandino G. Mutant p53: an oncogenic transcription factor. Oncogene. 2007; 26: 2212-9.
15 Miled C, Pontoglio M, Garbay S, Yaniv M, Weitzman JB. A genomic map of p53 binding sites identifies novel *p53* targets involved in an apoptotic network. Cancer Res. 2005; 65: 5096-104.
16 Bates S, Rowan S, Vousden KH. Characterisation of human cyclin G1 and G2: DNA damage inducible genes. Oncogene. 1996; 13: 1103-9.
17 Burns TF, Samuels T, Winckler S, Korgaonkar C, Tompkins V, Horne MD, Quelle EE. Cyclin G1 has growth inhibitory activity linked to eh *ARF-Mdm2-p53* and *pRb* tumor suppressor pathways. Mol Cancer Res. 2003; 1: 195-205.
18 Menendez D, Inga A, Resnick MA. The biological impact of the human master regulator *p53* can be altered by mutations that change the spectrum and expression of its target genes. Mol Cell Biol. 2006; 26: 2297-308.
19 Alvarez S, Drane P, Meiller A, Bras M, Deguin-Chambon V, Bouvard V, May E. A comprehensive study of *p53* transcriptional activity in thymus and spleen of gamma irradiated mouse: high sensitivity of genes involved in the two main apoptotic pathways. Int J Radiat Biol. 2006; 82: 761-70.
20 Gao C, Zou Z, Xu L, Moul J, Seth P, Srivastava S. *p53*-dependent induction of heat shock protein 27 (*HSP27*) expression. Int J Cancer. 2000; 88: 191-4.
21 Burns TF, Fei P, Scata KA, Dicker DT, El-Deiry WS. Silencing of the novel p53 target gene *Snk/Plk2* leads to mitotic catastrophe in paclitaxel-exposed cells, Mol Cell Biol. 2003; 23: 5556-71.
22 Lee JS, Chu IS, Mikaelyan A, Calvisi DF, Heo J, Reddy JK, Thorgeirsson SS. Application of comparative functional genomics to identify best-fit mouse models to study human cancer. Nat Genet. 2004; 36: 1306-11.
23 Meyer K, Lee JS, Dyck PA, Cao WQ, Rao MS, Thorgeirsson SS, Reddy JK. Molecular profiling of hepatocellular carcinomas developing spontaneously in acyl-CoA oxidase deficient mice: comparison with liver tumors induced in wild-type mice by a peroxisome proliferator and a genotoxic carcinogen. Carcinogenesis. 2003; 24: 975-84.
24 Moto M, Okamura M, Muguruma M, Ito T, Jin M, Kashida Y, Mitsumori K. Gene expression analysis on the dicyclanil-induced hepatocellular tumors in mice. Toxicol Pathol. 2006; 34: 744-51.
25 Hokaiwado N, Asamoto M, Tsujimura K, Hirota T, Ichihara T, Satoh T, Shirai T. Rapid analysis of gene expression changes caused by liver carcinogens and chemopreventive agents using a newly developed three-dimensional microarray system. Cancer Sci. 2004; 95: 123-30.
26 Kier LD, Neft R, Tang L, Suizu R, Cook T, Onsurez K, Tiegler K, Sakai Y, Orvitz, Nolan T. Sankar U, Li AP. Applications of microarrays with toxicologically relevant genes (tox genes) for the evaluation of chemical toxicants in Sprague Dawley rats *in vivo* and human hepatocytes

in vitro. Mutat Res. 2004; 549: 101-13.

27 Stahl S, Ittrich C, Marx-Stoelting P, Köhle C, Ott T, Buchmann A, Schwarz M. Effect of the tumor promoter phenobarbital on the pattern of global gene expression in liver of connexin32-wild-type and connexin32-deficient mice. Int J Cancer. 2005; 115: 861-9.

28 Deaciuc IV, Doherty DE, Burikhanov R, Lee EY, Stromberg AJ, Peng X, de Villiers WJ. Large-scale gene profiling of the liver in a mouse model of chronic, intragastric ethanol infusion. J Hepatol. 2004; 40: 219-27.

THE JOURNAL OF BIOLOGICAL CHEMISTRY VOL. 282, NO. 46, pp. 33507–33514, November 16, 2007

A New Role of Thrombopoietin Enhancing *ex Vivo* Expansion of Endothelial Precursor Cells Derived from AC133-positive Cells*

Received for publication, May 14, 2007, and in revised form, September 5, 2007 Published, JBC Papers in Press, September 7, 2007, DOI 10.1074/jbc.M703919200

Toshie Kanayasu-Toyoda[‡], Akiko Ishii-Watabe[‡], Takayoshi Suzuki[§], Tadashi Oshizawa[§], and Teruhide Yamaguchi[‡,1]

From the Divisions of [‡]Biological Chemistry and Biologicals, and [§]Cellular and Gene Therapy Products, National Institute of Health Sciences, Kamiyoga 1-18-1, Setagayaku, Tokyo 158-8501, Japan

We previously reported that CD31^{bright} cells, which were sorted from cultured AC133$^+$ cells of adult peripheral blood cells, differentiated more efficiently into endothelial cells than CD31$^+$ cells or CD31$^-$ cells, suggesting that CD31^{bright} cells may be endothelial precursor cells. In this study, we found that CD31^{bright} cells have a strong ability to release cytokines. The mixture of vascular endothelial growth factor (VEGF), thrombopoietin (TPO), and stem cell factor stimulated *ex vivo* expansion of the total cell number from cultured AC133$^+$ cells of adult peripheral blood cells and cord blood cells, resulting in incrementation of the adhesion cells, in which endothelial nitric oxide synthase and kinase insert domain-containing receptor were positive. Moreover, the mixture of VEGF and TPO increased the CD31^{bright} cell population when compared with VEGF alone or the mixture of VEGF and stem cell factor. These data suggest that TPO is an important growth factor that can promote endothelial precursor cells expansion *ex vivo*.

Neovascularization is an important adaptation to rescue tissue from critical ischemia. Postnatal blood vessel formation was formerly thought to be primarily due to the migration and proliferation of preexisting, fully differentiated endothelial cells, a process referred to as angiogenesis. Recent studies provide increasing evidence that circulating bone marrow-derived endothelial progenitor cells (EPCs)[2] contribute substantially to adult blood vessel formation (1–5). Cell therapy using EPCs is widely performed to rescue tissue damaged due to critical ischemia.

Although EPCs have been thought to be derived from many kinds of cells, cells characterized as CD34$^+$ (6), AC133$^+$ (7, 8), and CD14$^+$ (9) are also thought to differentiate to EPCs. The main role of EPCs has been thought to be the release of angiogenic factors such as interleukin-8 (IL-8), granulocyte colony-stimulating factor (G-CSF), hepatocyte growth factor, and vascular endothelial growth factor (VEGF) (9). To obtain a sufficient number of EPCs for the treatment may be very important in cell therapy for critical ischemia.

On the other hand, EPCs are mobilized from bone marrow by many substances such as G-CSF (10), granulocyte macrophage-colony stimulating factor (GM-CSF) (5), VEGF (3), erythropoietin (11–13), and statins (14, 15) *in vivo*. To get as many EPCs as possible without unduly burdening the patient, it is desirable to establish efficient expansion methods for EPCs *in vitro*.

Thrombopoietin (TPO), initially identified as the primary regulator of platelet production (16), plays an important and nonredundant role in the self-renewal of and expansion methods for hematopoietic stem cells (17–19). Recently, TPO has been found to exert a proangiogenic effect on cultured endothelial cells (20). The mechanism by which hematopoietic cytokines support revascularization *in vivo*, however, remains unknown. TPO has increased the number of colony-forming units-granulocyte-macrophage (21) and of burst-forming units-erythroid (22) *in vivo* and leads to a redistribution of colony-forming units-erythroid from marrow to spleen. Moreover, TPO acts in synergy with erythropoietin to increase the growth of burst-forming units-erythroid and the generation of colony-forming units-erythroid from marrow cells (21, 23, 24).

In our previous study (25), we isolated AC133$^+$ cells and examined their endothelial differentiation *in vitro*. CD31(PECAM-1)$^+$ and CD31^{bright} cells appeared at an early stage of the *in vitro* differentiation of AC133$^+$ cells, and CD31^{bright} cells derived from AC133$^+$ cells were identified as the precursors of endothelial cells because CD31^{bright} cells had differentiated more efficiently to endothelial cells than others. Therefore, we conclude that CD31^{bright} cells derived from AC133$^+$ cells possess the typical character of EPCs. In this study, we analyzed the effects of TPO on the appearance of CD31^{bright} cells from AC133$^+$ cells, and we show that TPO plays an important role in *in vitro* EPC expansion.

EXPERIMENTAL PROCEDURES

Reagents—Recombinant TPO and recombinant stem cell factor (SCF) were kindly provided by Kirin-Amgen Inc. (Thousand Oaks, CA). Recombinant human VEGF was purchased from Strathmann Biotec AG (Hamburg, Germany). The AC133

* This work was supported in part by a grant-in-aid for health and labor science research from the Japanese Ministry of Health, Labor, and Welfare, and in part by a grant-in-aid for Research on Health Sciences focusing on Drug Innovation from the Japan Health Sciences Foundation. The costs of publication of this article were defrayed in part by the payment of page charges. This article must therefore be hereby marked "*advertisement*" in accordance with 18 U.S.C. Section 1734 solely to indicate this fact.

[1] To whom correspondence should be addressed. Tel.: 81-3-3700-9064; Fax: 81-3-3707-6950; E-mail: yamaguch@nihs.go.jp.

[2] The abbreviations used are: EPCs, endothelial precursor cells; VEGF, vascular endothelial growth factor; FN, fibronectin; PBS, phosphate-buffered saline; FITC, fluorescein isothiocyanate; PE, phycoerythrin; TPO, thrombopoietin; SCF, stem cell factor; G-CSF, granulocyte colony-stimulating factor; GM-CSF, granulocyte macrophage-colony stimulating factor; IL, interleukin; PI3K, phosphatidylinositol 3-kinase; VEcad, vascular endothelial cadherin; eNOS, endothelial nitric oxide synthase; FBS, fetal bovine serum; STAT, signal transducers and activators of transcription; JAK, Janus kinase; KDR, kinase insert domain-containing receptor.

magnetic cell sorting kit and phycoerythrin (PE)-conjugated anti-CD133/2 antibody were from Miltenyi Biotec (Gladbach, Germany). Allophycocyanin-conjugated anti-CD110 (TPO receptor) antibody, fluorescein isothiocyanate (FITC)-conjugated anti-CD31 monoclonal antibody, FITC-conjugated anti-CD34 monoclonal antibody, and anti-STAT3 monoclonal antibody were from Pharmingen. Phycoerythrin-conjugated vascular endothelial cadherin (VEcad/CD144) antibody was from Beckman Coulter (Marseilles, France). Anti-vascular endothelial growth factor receptor-2 (Flk-1/KDR) monoclonal antibody (Santa Cruz Biotechnology, Inc., Santa Cruz, CA) and anti-human endothelial nitric oxide synthase (eNOS) rabbit polyclonal antibody (Cayman Chemical, Ann Arbor, MI) were obtained. Anti-phospho-Akt (Ser-473) antibody, anti-Akt antibody, and anti-phospho-STAT3 (Tyr-705) antibody were from Cell Signaling Technology (Beverly, MA). Fibronectin (FN)- and type IV collagen-coated dishes were purchased from Iwaki Co., Tokyo, Japan. Phycoerythrin-conjugated anti-CD14 antibody was from DakoCytomation (Glostrup, Denmark).

Preparation of Peripheral Blood Mononuclear Cells—Human cord blood was kindly supplied by the Metro Tokyo Red Cross Cord Blood Bank (Tokyo, Japan) with informed consent. The buffy coat fraction was prepared from voluntary donated human blood of Saitama Red Cross of Japan (Saitama, Japan). The blood sample was diluted with phosphate-buffered saline (PBS) containing 2 mM EDTA and was loaded on a Lymphoprep™ tube (Axis-Shield PoC AS, Oslo Norway) (density = 1.077). After being centrifuged for 20 min 800 × *g* at 18 °C, mononuclear cells were collected and washed with sorting solution (PBS supplemented with 2 mM EDTA and 0.5% bovine serum albumin).

Flow Cytometric Analysis of AC133 and CD34 Expression in Mononuclear Cells—To eliminate the dead cells, dead cells were stained with 7-amino actinomycin D. Mononuclear cells were labeled with PE-conjugated anti-AC133 monoclonal antibody and FITC-conjugated anti-CD34 monoclonal antibody simultaneously at 4 °C for 30 min. After washing with the sorting solution, flow cytometric analysis was performed with a FACSCalibur (BD Biosciences).

Magnetic Cell Sorting of AC133$^+$ Cells—Mononuclear cells were labeled with magnetic bead-conjugated anti-AC133 antibodies according to the protocol directed by the manufacturer. After the brief wash with the sorting solution, the cells were separated by a magnetic cell separator (autoMACS, Miltenyi Biotec, Gladbach, Germany), and the positive cells were then collected.

Culture of AC133$^+$ Cells—Isolated AC133$^+$ cells were cultured in EBM-2 (Cambrex Corp., East Rutherford, NJ) medium containing 20% heat-inactivated FBS and 30 mg/liter kanamycin sulfate at 37 °C under moisturized air containing 5% CO_2 with 50 ng/ml VEGF as control medium. Control medium containing VEGF was added with TPO, SCF, or both. Cells were plated on FN- or type IV collagen-coated dishes at a cell density of ~10^6 cells/ml. We have previously shown that EPCs can tightly adhere to an FN-coated dish but weakly to type IV collagen-coated dish (25). Analysis of adherent EPCs was performed on FN-coated dish and that of suspended EPCs on type IV collagen-coated dish. Half of the medium was exchanged once every 3–4 days with fresh medium. Adherent cells on FN-coated dish were fixed with ethanol chilled to −20 °C and then subsequently subjected to an immunostaining procedure or other treatments. Cells on type IV collagen-coated dish were subsequently subjected to flow cytometric analysis.

Immunostaining of Adherent Cells—After fixation with chilled ethanol (−20 °C), the cell layer was washed three times with PBS. Cells were incubated with 1% bovine serum albumin in PBS (−) for 1 h at 4 °C for blocking and then with each first antibody in 1% bovine serum albumin in PBS (−) for 1 h at 4 °C. After washing with PBS, the cells were incubated with FITC-conjugated anti-mouse IgG antibody or rhodamine-conjugated anti-rabbit IgG antibody for 1 h at 4 °C. Cells were washed with PBS and then examined using a Zeiss LSM 510 microscope with an excitation wavelength of 488 nm and an emission of 530/30 nm for FITC or 570/30 nm for rhodamine.

In every experiment, we used nonspecific immunoglobulin corresponding to the first antibody species as a control and confirmed that the cells were not stained with control immunoglobulin. The fluorescence intensity of 20 randomly selected cells was calculated using the Scion Image program within the linear range for quantitation.

Analysis of Cytokines in the Supernatant of CD31^{bright} and CD31$^+$ Cells—The expression of CD31 on cultured AC133$^+$ cells was determined with a flow cytometer. After AC133$^+$ cells were cultured for several days on either FN-coated or collagen type IV-coated dishes, both adherent and nonadherent cells were collected. The collected cells were labeled with FITC-labeled anti-CD31 antibody for 15 min at 4 °C. After a brief wash with 0.5% bovine serum albumin in PBS, flow cytometric analysis was performed. CD31^{bright} and CD31$^+$ cells were sorted from cultured AC133$^+$ cells with FACSAria (BD Biosciences). Sorted cells of both populations were subsequently cultured in EBM-2 supplemented with 20% FBS in the absence of any cytokines. After 5 days, the collected supernatant of cells was frozen at −20 °C. Cytokines were measured by a BD™ cytometric beads array Flex set system (BD Biosciences) according to the manufacturer's protocol.

Flow Cytometric Analysis of Various Cell Surface Markers in Cultured AC133$^+$ Cells—After AC133$^+$ cells were cultured for the indicated period, cells were co-stained with FITC-labeled anti-CD31 antibody and PE-labeled anti-CD14 antibody or PE-labeled VEcad antibody. Cells were also stained with FITC-labeled anti-CD31 antibody, allophycocyanin-labeled anti-CD110 antibody, and PE-labeled anti-AC133 antibody triply and then subjected to flow cytometry. Dead cells were eliminated by staining with 7-amino actinomycin D.

Calculation of the Absolute Number of CD31^{bright} Cells—The absolute number of CD31^{bright} cells was multiplied by the total cell number of each well, and the ratio of CD31^{bright} cells was analyzed by fluorescence-activated cell sorter.

Preparation of Cell Lysates and Immunoblotting—After cell sorting, AC133$^+$ cells were suspended in 20% FBS-EBM2 and cultured for 3 days in the presence of VEGF and TPO. Cells were collected and incubated in 2% FBS-EBM2 for 1 h. Cells were stimulated by 50 ng/ml TPO, 50 ng/ml VEGF, or both for 15 min. Cells (1 × 10^6) were collected and lysed in lysis buffer containing 1% Triton X-100, 10 mM K_2HPO_4/KH_2PO_4 (pH

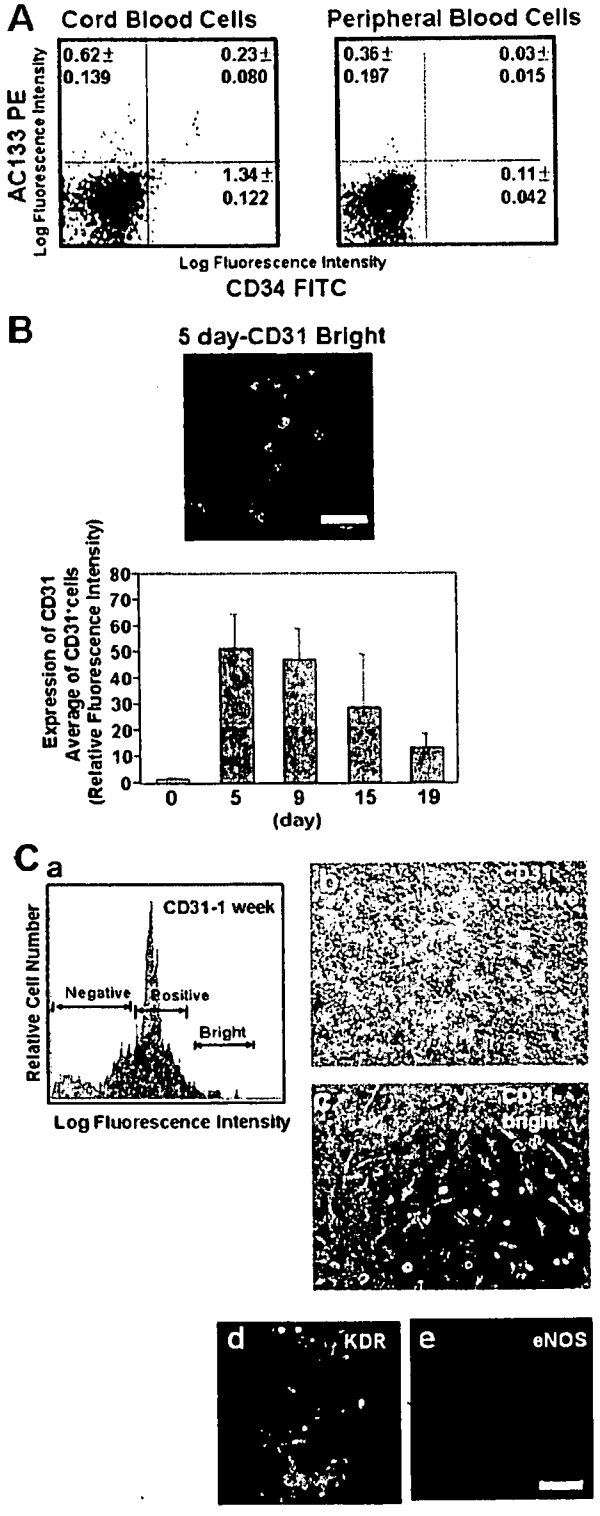

FIGURE 1. ***In vitro* differentiation of AC133$^+$ cells of cord blood into endothelial cells.** *A*, expression of AC133 and CD34 cells in human cord blood and peripheral blood mononuclear cells was analyzed by staining with AC133-PE (*vertical axis*) and CD34-FITC (*horizontal axis*). The *numbers* in the flow cytometric dot blots indicates the percentage of each population ± S.D. *B*, when AC133$^+$ cells were cultured for 19 days in the presence of VEGF on FN-coated dishes, the appearance of CD31$^+$ cells was analyzed. The *upper panel* shows the fluorescent photomicrograph of adhesion cells stained with FITC-conjugated anti-CD31 antibody after a 5-day culture. Quantitation of the fluorescence intensity of 20 CD31-positive cells was analyzed as described under "Experimental Procedures." Columns and bars represent the means ± S.D. from 20 cells (*B*, *lower panel*). *C*, the CD31-negative, positive, and bright cell populations prepared after 1-week cultivation of AC133$^+$ cells are shown in a representative histogram stained with FITC-conjugated anti-CD31 antibody. The *x* axis represents the log fluorescence intensity of CD31-FITC, *y* axis relative cell number (*panel a*). *Panels b* and *c* show phase-contrast microscopic photographs of cultured CD31-positive and bright cells, respectively, subsequently cultured for 1 week after cell sorting. The *bottom panels d* and *e* show the fluorescent photomicrographs of adhesion cells from the CD31^{bright} fraction stained with anti-KDR antibody and anti-eNOS antibody, respectively. *Scale bar*, 100 μm.

7.5), 1 mM EDTA, 5 mM EGTA, 10 mM $MgCl_2$, and 50 mM β-glycerophosphate, along with 1/100 (v/v) protease inhibitor mixture (Sigma) and 1/100 (v/v) phosphatase inhibitor mixture (Sigma). The cellular lysate of 5×10^5 cells/lane was subjected to Western blotting analysis.

Statistical Analysis—Statistical analysis was performed using the unpaired Student's *t* test, and the dose response of TPO was compared between the four groups by one-way analysis of variance and the Tukey test using Prism 4 software. Values of $p < 0.05$ were considered to indicate statistical significance. Each experiment was repeated three times, and the representative data are indicated.

RESULTS

We previously reported that during the *in vitro* differentiation of peripheral blood AC133$^+$ cells into the endothelial cells, the expression of CD31 was the earliest marker among all of the tested markers (25). Moreover, by analyzing the ability of differentiation into endothelial cells, CD31^{bright} cells were shown to exhibit EPC character when compared with the CD31$^+$ fraction. Since cord blood is a rich source of blood stem cells such as CD34$^+$ and AC133$^+$ cells, it is expected to be a useful source for CD31^{bright} cells. At first, we attempted to determine whether the CD31^{bright} fraction derived from cord blood AC133$^+$ cells contained EPCs. As shown in Fig. 1*A*, the populations of AC133$^+$ CD34$^-$ cells, AC133$^-$ CD34$^+$ cells, and AC133$^+$ CD34$^+$ cells in cord blood were approximately four times greater than those in peripheral blood (Fig. 1*A*). After 5 days of cultivation of AC133$^+$ cells on an FN-coated dish, adherent CD31-positive cells were observed (Fig. 1*B*, *upper panel*). Analysis of the fluorescence intensity of CD31-positive cells revealed that the average fluorescence intensity in CD31$^+$ cells was highest on day 5 (Fig. 1*B*, *lower panel*), corresponding to the results of peripheral blood cells.

After 1 week of cultivation of AC133$^+$ cells on a collagen type IV-coated dish, on which cells adhered more loosely when compared with the FN-coated dish, cells were collected and sorted into CD31$^+$ and CD31^{bright} fractions, as shown in Fig. 1*C*, *panel a*, and both cell types were cultured on an FN-coated dish for 1 week after the sorting. The number of cells adhering and spreading was higher in the CD31^{bright} fraction (Fig. 1*C*, *panel c*) than in the CD31$^+$ fraction (Fig. 1*C*, *panel b*), and these adhering cells are apparently KDR- (Fig. 1*C*, *panel d*) and eNOS-positive (Fig. 1*C*, *panel e*). The large areas of intense green fluorescence represent the colonies of CD31^{bright} cells. These data indicate that CD31^{bright} cells derived from AC133$^+$ cells of both peripheral blood and cord blood are EPCs.

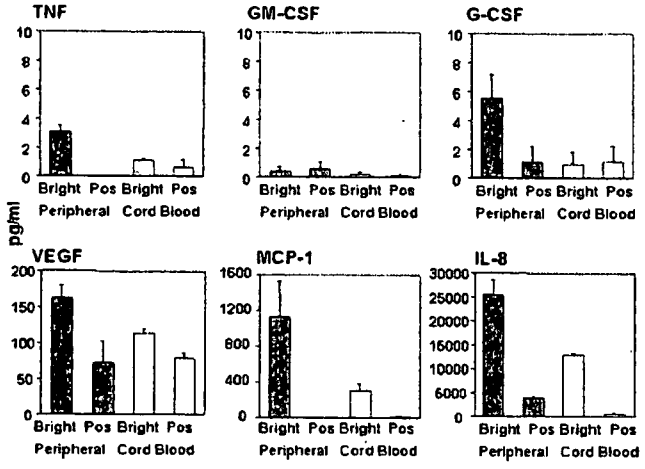

FIGURE 2. **Various cytokines released from CD31$^+$ cells and CD31^{bright} cells.** Production of various cytokines from CD31$^-$ cells and CD31^{bright} cells derived from AC133$^+$ cells cultivated for 5 days was measured. *Gray columns* indicate the cytokine production by cells from peripheral blood and open columns from cord blood. Columns and bars represent the means ± S.D. from three separate experiments. *TNF*, tumor necrosis factor; *Pos*, positive; *MCP-1*, monocyte chemoattractant protein-1.

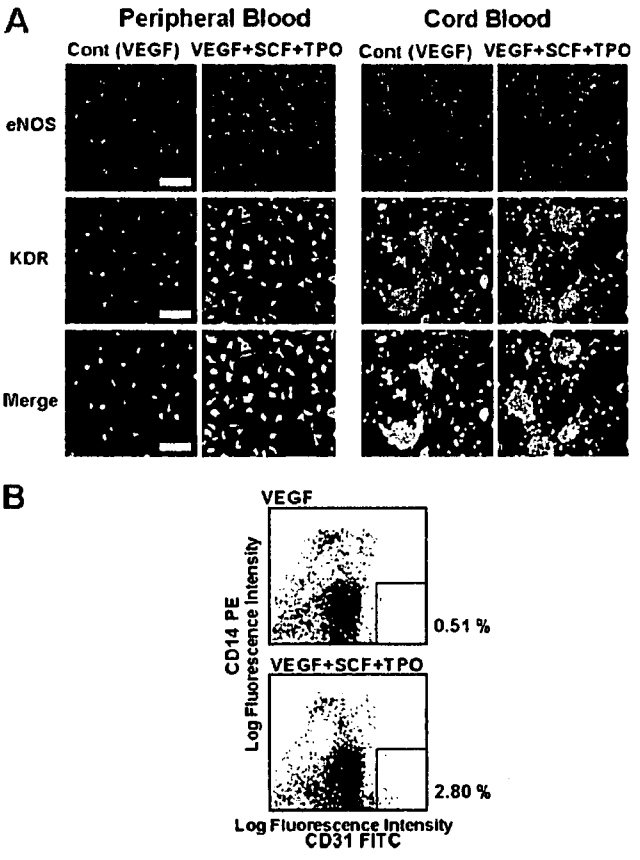

FIGURE 3. **Increment of EPCs from AC133$^+$ cells in the presence of TPO and SCF.** *A*, AC133$^+$ cells were differentiated for 2 weeks in the presence of either VEGF alone or the combination of TPO, SCF, and VEGF on an FN-coated dish. The *upper* and *middle panels* indicate the fluorescent photomicrographs of cells stained with anti-eNOS antibody and anti-KDR antibody, respectively. The *bottom panels* indicate the merged images of both antibodies. From the *left side*, control (*Cont*) and the mixture of peripheral blood, control, and the mixture of cord blood. *Scale bar*, 100 μm. *B*, CD14 and CD31 expression in cultured AC133$^+$ cells for 1 week was stained with CD14-PE (*vertical axis*) and CD31-FITC (*horizontal axis*). The *upper panel* indicates cells treated with VEGF alone, and the *lower panel* indicates cells treated with the mixture of VEGF, SCF, and TPO. The *number* on the *right side* of the flow cytometric dot blot indicates the percentage of the CD14$^-$ CD31^{bright} population.

Several reports have shown that EPCs produce cytokines (9, 26, 27), but the ability of CD31$^+$ or CD31^{bright} cells derived from AC133$^+$ cells to produce cytokines is not known. After cell sorting, quantitative analysis of cytokines released by CD31$^+$ cells and CD31^{bright} cells was carried out at 5 days after the cultivation. As shown in Fig. 2, IL-8 was markedly produced by CD31^{bright} cells from both peripheral blood and cord blood when compared with CD31$^+$ cells. The production of monocyte chemoattractant protein-1 (MCP-1) by CD31^{bright} cells was also higher than that of CD31$^+$ cells. The production of VEGF was higher by CD31^{bright} cells than by CD31$^-$ cells but not significantly. The production of all cytokines by CD31^{bright} cells from peripheral blood was higher than that from cord blood. Tumor necrosis factor-α, GM-CSF, and G-CSF were hardly produced by CD31^{bright} and CD31$^+$ cells. These data indicate that CD31^{bright} cells derived from AC133$^+$ cells have a strong ability to produce chemokines.

It has been reported that TPO and SCF are potent stimulators of multipotent cell proliferation (17, 19). Next, the effects of both growth factors on EPC growth and differentiation in our culture system were determined. After the addition of both TPO and SCF for 2 weeks, the expression of eNOS and KDR in adhered cells was analyzed (Fig. 3*A*). Fig. 3*A* clearly indicates that AC133$^+$ cells from both peripheral blood and cord blood differentiate into eNOS$^+$ and KDR$^+$ cells more efficiently in the presence of the mixture of TPO, SCF, and VEGF than of VEGF alone. Flow cytometric analysis revealed that the ratio of CD31^{bright} CD14$^-$ cells increased in the presence of the mixture of TPO, SCF, and VEGF when AC133$^+$ cells were cultured on collagen type IV-coated dish for 1 week (Fig. 3*B*).

We next examined which growth factor is dominant in the induction and proliferation of CD31^{bright} cells. The total cell number of cultured AC133$^-$ cells from both peripheral blood (Fig. 4*A*, *upper panel*) and cord blood (Fig. 4*A*, *lower panel*) significantly increased in the presence of TPO, SCF, or both growth factors when compared with that of VEGF alone during a 1-week period. As shown in Fig. 4*B*, however, the increment in the ratio of the CD31^{bright} cell population was observed only in the presence of TPO. The absolute number of CD31^{bright} cells, calculated by the total cell number and the ratio of the CD31^{bright} cell population, was markedly increased by TPO (Fig. 4*C*). In contrast, SCF induced the increase in total cell number to the same level as TPO (Fig. 4*A*), but it did not induce the increase in either the ratio of the CD31^{bright} cell population (Fig. 4*B*) or the number of CD31^{bright} cells (Fig. 4*C*). Next, we examined whether TPO and VEGF can synergistically affect the induction of CD31^{bright} cells during a 1-week cultivation. As shown in Fig. 4*D*, although VEGF had no effects on the total cell number (Fig. 4*D*, *panel a*), it increased the ratio of the CD31^{bright} cell population to 1.4-fold higher than that of the control (Fig. 4*D*, *panel b*), resulting in a slight increase in the number of CD31^{bright} cells (Fig. 4*D*, *panel c*). Thrombopoietin alone induced an increase in not only the total cell number (Fig. 4*D*, *panel a*) but also the ratio of the CD31^{bright} cell population (Fig. 4*D*, *panel b*), resulting in an ~24-fold increment of the absolute

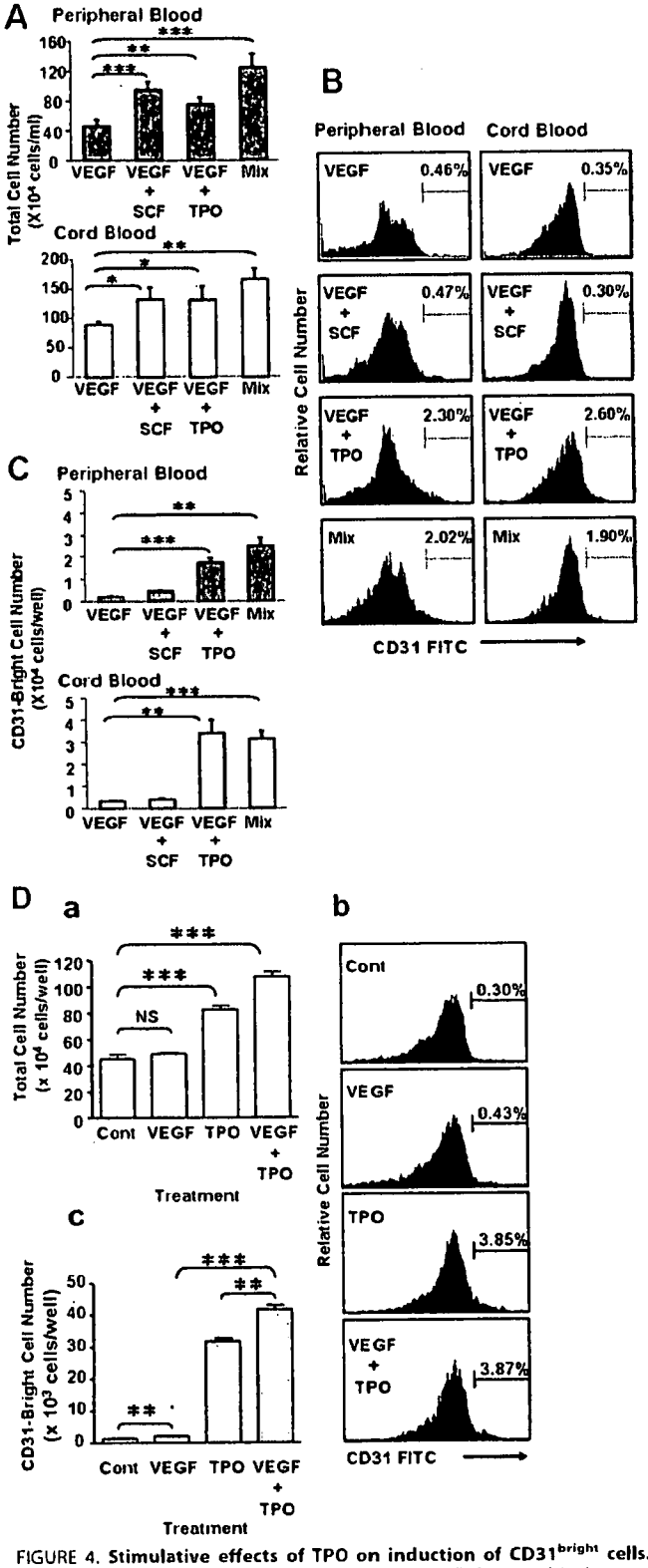

FIGURE 4. **Stimulative effects of TPO on induction of CD31^{bright} cells.** *A*, alteration of the cell number of cultivated AC133$^-$ cells for 1 week in the combination of growth factors. *Mix*, VEGF + SCF + TPO. *B*, the flow cytometric histogram of AC133$^+$-derived cells stained with FITC-labeled anti-CD31 antibody after a 1-week culture. The *representing number* in the flow cytometric histogram indicates the percentage of the CD31^{bright} cell population. The *left panels* are peripheral blood, and the *right panels* are cord blood. *C*, CD31^{bright} cells numbers were calculated by both the total cell number and the ratio the of CD31^{bright} population. *D*, the effects of TPO alone on EPC differentiation derived from AC133$^+$ cells of cord blood. The *upper left panel* (*a*) shows the total cell number after a 1-week culture, the *right panels* (*b*) show the flow cytometric histogram of AC133$^-$-derived cells stained with FITC-labeled anti-CD31 antibody, and the *lower left panel* (*c*) shows the calculated CD31^{bright} cell number. Columns and bars represent the means ± S.D. (*, $p < 0.05$; **, $p < 0.01$; ***, $p < 0.001$). *NS*, not significant; *Cont*, control.

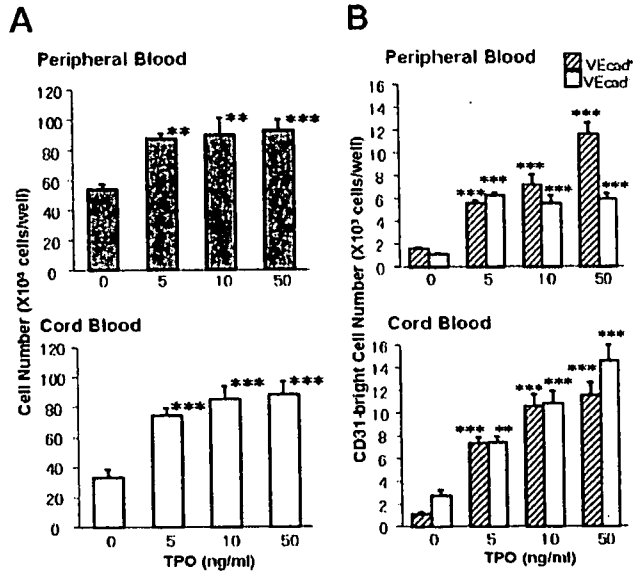

FIGURE 5. **Dose-dependent effects of TPO on the induction of CD31^{bright} cells from AC133$^+$ cells.** AC133$^+$ cells were treated with various concentrations of TPO for 1 week. The *left panels* (*A*) are the total cell number of cultured AC133$^+$ cells from peripheral blood (*upper panel*) and cord blood (*lower panel*). The *right panels* (*B*) are the calculated CD31^{bright} cell number from peripheral blood (*upper panel*) and cord blood (*lower panel*). Columns and bars represent the means ± S.D. (**, $p < 0.01$; ***, $p < 0.001$). *Striped* and *dotted columns* represent CD31^{bright}VEcad$^-$ cells and CD31^{bright}VEcad$^-$ cells, respectively.

number of CD31^{bright} cells when compared with the control (Fig. 4*D*, *panel c*). The concomitant treatment with both VEGF and TPO showed a synergic increase in the number of CD31^{bright} cells (Fig. 4*D*, *panel c*).

When AC133$^+$ cells were cultured with various concentrations of TPO in the presence of constant concentrations of VEGF (50 ng/ml), the total cell number from both peripheral blood (Fig. 5*A*, *upper panel*) and cord blood (Fig. 5*A*, *lower panel*) significantly increased at 5 ng/ml of TPO when compared with the control, and there was no significant difference in the total cell number from 5 to 50 ng/ml of TPO. However, TPO increased the ratio of CD31^{bright} cells of flow cytometry dose-dependently as follows: control, 0.50%; 5 ng/ml, 1.36%; 10 ng, 1.42%; 50 ng/ml 1.90% in peripheral blood and control, 1.16%; 5 ng/ml, 1.99%; 10 ng, 2.51%; 50 ng/ml 2.96% in cord blood. TPO markedly induced the differentiation of AC133$^+$ cells into CD31^{bright}VEcad$^+$ cells in the case of both peripheral blood (Fig. 5*B*, *upper panel*) and cord blood (Fig. 5*B*, *lower panel*) in a dose-dependent manner. In the case of cord blood cells, differentiation into CD31^{bright}VEcad$^-$ cells was also induced by TPO.

The effects of TPO on total cell number during 6-day culture of AC133$^+$ cells were determined. Although the total cell num-

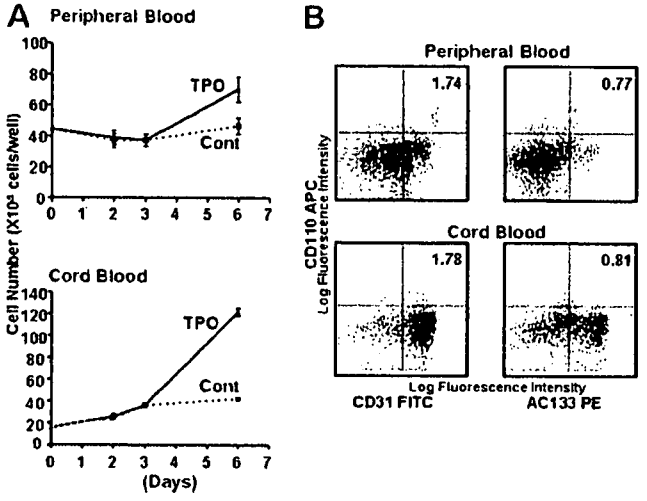

FIGURE 6. **Time-course analysis of TPO-treated AC133$^+$ cells and expression of TPO receptor (CD110).** *A*, alteration of cell number was counted at 2, 3, and 6 days. *Solid* and *dotted lines* indicate TPO-treated cells and control ((*Cont*) VEGF alone) cells, respectively. The results represent mean ± S.E. of triplicate wells. *B*, flow cytometric analysis of CD110 expression on AC133$^+$ cells cultured for 3 days was carried out. The *y axis* represents the log fluorescence intensity of CD110-allophycocyanin (*APC*), and the *x axis* represents that of CD31-FITC (*left panels*) and AC133-PE (*right panels*). The *number* in the flow cytometric dot blot indicates the percentage of CD110$^+$ CD31$^+$ and CD110$^+$ AC133$^+$ populations, respectively. The *upper panels* are peripheral blood, and the *lower panels* are cord blood.

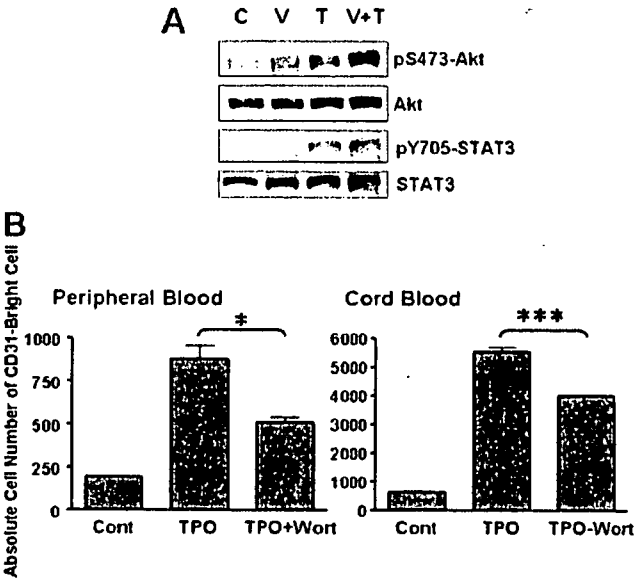

FIGURE 7. **Analysis of TPO-induced signal transduction on AC133$^+$ cells of cord blood.** *A*, activation of Akt or STAT3 was analyzed by Western blotting with anti-phospho-specific Ser-473-Akt antibody (*top panel*) and reprobed with anti-Akt antibody (*second panel*), or with anti-phospho-specific Tyr-705-STAT3 antibody (*third panel*) and reprobed with anti-STAT3 antibody (*lower panel*) after stimulation by VEGF, TPO, or both VEGF and TPO for 15 min using 3-day-cultured AC133$^+$ cells. *C*, control; *V*, VEGF; *T*, TPO. *B*, the effects of wortmannin on CD31^{bright} cell induction were investigated. The *right panel* shows peripheral blood, and the *left panel* shows cord blood. The *y axis* represents the CD31^{bright} cell number. *Wort*, 100 nM wortmannin. Columns and bars represent the means ± S.E. (*, $p < 0.05$; ***, $p < 0.001$). *Cont*, control.

ber from AC133$^+$ cells slightly and constantly increased from day 0 to day 6 in the absence of TPO, total cells markedly increased after the third day in the presence of TPO (Fig. 6*A*). Next, the alternation of TPO receptor (CD110) expression was analyzed during the cultivation of AC133$^+$ cells. Although the percentages of both AC133$^+$ CD110$^+$ cells and CD31$^+$ CD110$^+$ cells were 0% just after magnetic cell sorting, 3 days after the cultivation, ~2% of CD31$^+$ CD110$^+$ cells (Fig. 6*B*, *left panel*) and 1% of AC133$^+$ CD110$^+$ cells (Fig. 6*B*, *right panel*) appeared from AC133$^+$ cells in the peripheral blood and cord blood, respectively. These data indicate the possibility that sorted AC133$^+$ cells may differentiate into AC133$^+$ CD110$^+$ cells and may subsequently proliferate and differentiate into EPCs in response to TPO.

It has been reported that TPO activates the PI3K/Akt pathway (28) or JAK/STAT pathway (20, 29, 30) in target cells. In addition, in the present study, TPO induced a marked proliferation of AC133$^+$ cells after 3-day culture, and CD110 expression in cells cultured for 3 days from both cord blood and peripheral blood was also observed (Fig. 6, *A* and *B*). We then attempted to determine whether TPO activates Akt or STAT in AC133$^+$ cells cultured for 3 days by analyzing the phosphorylation at Ser-473 of Akt or the phosphorylation at Tyr-705 of STAT3, which are the active forms of Akt or STAT3, respectively. As shown in Fig. 7*A*, phosphorylation at Ser-473 of Akt was stimulated by both VEGF and TPO at 15 min and was more markedly stimulated by concomitant treatment with VEGF and TPO than by a single treatment (Fig. 7*A*, *top panel*). Phosphorylation at Tyr-705 of STAT3 was observed only in the presence of TPO, and unlike in the phosphorylation at Ser-473 of Akt, an increased amount of phosphorylation was not observed in the concomitant presence of VEGF and TPO (Fig. 7*A*, *third panel*). On the other hand, there was no difference in the expression of Akt and STAT3 protein levels (Fig. 7*A*, *second panel* and *bottom panel*, respectively). The induction of CD31^{bright} cells was not perfectly but significantly inhibited by wortmannin, an inhibitor of PI3K, suggesting that the PI3K/Akt pathway plays an important role in TPO-induced EPC differentiation (Fig. 7*B*).

DISCUSSION

We have previously reported that CD31^{bright} cells derived from AC133$^+$ cells in human peripheral blood are EPCs (25). In the present study, CD31^{bright} cells also appeared from AC133$^+$ cells prepared from cord blood, which are a rich source of stem cells during the early period of cultivation (Fig. 1, *A* and *B*). When cells were separated in terms of CD31 expression (Fig. 1*C*), CD31^{bright} cells differentiated into KDR-positive and eNOS-positive adherent cells. These data indicate that CD31^{bright} cells derived from AC133$^+$ cells in cord blood have some characteristics similar to those of EPCs in peripheral blood. Although these EPCs in both cord blood and peripheral blood could not form tube-like structure by themselves on Matrigel (data not shown), they secreted angiogenic growth factors (Fig. 2) such as VEGF, IL-8 (31, 32), and monocyte chemoattractant protein-1 (MCP-1) (33). It has been reported that there are at least two types of EPCs: early EPCs and late EPCs. Early EPCs are unable to form tube-like structures and secrete VEGF and IL-8 showing peak growth at 2–3 weeks (9, 26, 27). Late EPCs with the ability to proliferate and having a cobblestone shape appear late at 2–3 weeks, show exponential growth at 4–8 weeks, and have the ability to form tube-like structures

(26, 27, 34). Rehman *et al.* (9) have reported that EPCs derived from monocytes/macrophages do not proliferate but instead release potent proangiogenic growth factors. In many studies (9, 26, 27, 35–37), because the origin of early EPCs was $CD14^+$ cells or was not precluded by monocytic cells, CD14 expression was still observed in the EPCs after cultivation. In our study, in which $AC133^+$ cells were used as the origin of the EPCs, CD14 expression was not observed in $CD31^{bright}$ cells induced by TPO (Fig. 3*B*). Although the $CD31^{bright}$ cells identified as EPCs in this report and in a previous report did not correspond to their cells in terms of the origin of the cells or cell surface markers, these cells may be early EPCs that can release potent proangiogenic growth factors (Fig. 2). In any event, EPCs are thought to be a heterogeneous population, unlike late EPCs, which have a high ability to proliferate.

Circulating EPCs are up-regulated under physiological or pathological conditions and also by 3-hydroxy-3-methyl-glutaryl-CoA reductase inhibitors (14, 15) and cytokines such as erythropoietin (11–13) and G-CSF (10). In this report, we have revealed the possibility of marked expansion of EPCs *in vitro* by TPO. Brizzi *et al.* (20) have reported that TPO directly stimulates endothelial cell motility and neoangiogenesis. In the present study, TPO may have played a stimulatory role in the differentiation of EPCs from circulating stem cells.

Although both TPO and SCF have the same potency with regard to proliferation of $AC133^+$ cells (Fig. 4*A*), TPO specifically induces an increase in the ratio of the $CD31^{bright}$ cell population when compared with SCF (Fig. 4, *B* and *C*). To develop useful cell therapy products for severe ischemia, it has been considered desirable to establish the efficient expansion of EPCs *in vitro*. Thrombopoietin could increase $CD31^{bright}$ cells (EPCs) even in the absence of VEGF. Kirito *et al.* (38) have reported that TPO enhances expression of VEGF in hematopoietic cells through induction of hypoxia-inducible factor 1α. These observations suggest the possibility that the production of EPCs by TPO may be supported by VEGF produced by $AC133^+$ cells. However, from the perspective that TPO and VEGF have synergistic effects on the induction of EPCs, TPO seems to induce EPCs through another signaling cascade.

Thrombopoietin is a major regulator of the proliferation, differentiation, and maturation of megakaryocytes (39, 40). The results from recent studies suggest that TPO can act not only as a lineage-specific hematopoietic growth factor but also can affect other hematopoietic cell types. For example, TPO alone does not induce proliferation of long term repopulating hematopoietic stem cells. However, in combination with SCF or IL-3, TPO has several synergistic effects on cell proliferation (19). Our results have revealed a new role of TPO in the production of EPCs.

In the process of differentiation of $AC133^+$ cells into $CD31^{bright}$ cells, both peripheral blood and cord blood appear to be very similar. $AC133^+$ cells of cord blood, however, have a stronger ability to proliferate than those of peripheral blood (Fig. 6*A*). Moreover, TPO stimulates the induction of $CD31^{bright}VEcad^-$ cells only from cord blood (Fig. 5*B*) at high concentrations. Hur *et al.* (26) have reported that $VEcad^-$ EPCs are thought to be an early EPC. It is therefore thought that $AC133^+$ cells of cord blood are more immature than those of peripheral blood.

Although the total cell number treated with TPO slightly increased in a dose-dependent manner (Fig. 5*A*), the $CD31^{bright}$ cell number markedly increased as the TPO concentration increased (Fig. 5*B*). These data suggest the possibility that a higher concentration of TPO may be needed for $CD31^{bright}$ cell induction from $AC133^+$ cells.

When $AC133^+$ cells were stimulated by TPO or VEGF, an increase in the phosphorylation of Akt at Ser-473 was observed. This increase was strongly enhanced by concomitant treatment with VEGF and TPO (Fig. 7*A*). The induction of $CD31^{bright}$ cells by these growth factors (Fig. 4*D*) was consistent with the increase in the phosphorylation of Akt at Ser-473. TPO but not VEGF could also stimulate the phosphorylation of STAT3 at Tyr-705. We previously reported that the PI3K/p70 S6 kinase pathway and the JAK/STAT3 pathway were important for proliferation and differentiation, respectively, in neutrophilic differentiation (41, 42). Owing to the stimulation of both the PI3K/Akt and the JAK/STAT pathways, we postulated that TPO may be a stronger stimulator of EPC production than VEGF. As shown in Fig. 7*B*, however, wortmannin could not completely inhibit the induction of $CD31^{bright}$ cells. Therefore, a pathway other than the PI3K/Akt pathway may also work for the proliferation and differentiation of EPCs.

The observation of unfavorable angiogenesis has recently been reported after transplantation of bone marrow mononuclear cells in patients with thromboangiitis obliterans (43). Moreover, transfer of both spleen cell-derived EPCs and bone marrow mononuclear cells accelerate atherosclerosis in apoE knockout mice, whereas EPC transfer reduces markers associated with plaque stability (44). These observations suggest that transplantation of differentiated cells from EPCs may be useful therapy as regenerative medicine.

In conclusion, we have demonstrated a new role of TPO in enhancing the differentiation of $AC133^+$ cells into $CD31^{bright}$ cells (EPCs) *in vitro*. These findings may contribute to further development of cell therapy for critical ischemia.

Acknowledgments—We thank Saitama Red Cross of Japan (Saitama, Japan) and Metro Tokyo Red Cross Cord Blood Bank (Tokyo, Japan) for their kind cooperation. We also thank Kirin-Amgen Inc. for their kind gift of recombinant TPO and recombinant SCF.

REFERENCES

1. Asahara, T., Masuda, H., Takahashi, T., Kalka, C., Pastore, C., Silver, M., Kearne, M., Magner, M., and Isner, J. M. (1999) *Circ. Res.* **85**, 221–228
2. Asahara, T., Murohara, T., Sullivan, A., Silver, M., van der Zee, R., Li, T., Witzenbichler, B., Schatteman, G., and Isner, J. M. (1997) *Science* **275**, 964–967
3. Asahara, T., Takahashi, T., Masuda, H., Kalka, C., Chen, D., Iwaguro, H., Inai, Y., Silver, M., and Isner, J. M. (1999) *EMBO J.* **18**, 3964–3972
4. Shi, Q., Rafii, S., Wu, M. H., Wijelath, E. S., Yu, C., Ishida, A., Fujita, Y., Kothari, S., Mohle, R., Sauvage, L. R., Moore, M. A., Storb, R. F., and Hammond, W. P. (1998) *Blood* **92**, 362–367
5. Takahashi, T., Kalka, C., Masuda, H., Chen, D., Silver, M., Kearney, M., Magner, M., Isner, J. M., and Asahara, T. (1999) *Nat. Med.* **5**, 434–438
6. Nieda, M., Nicol, A., Denning-Kendall, P., Sweetenham, J., Bradley, B., and Hows, J. (1997) *Br. J. Haematol.* **98**, 775–777
7. Gill, M., Dias, S., Hattori, K., Rivera, M. L., Hicklin, D., Witte, L., Girardi, L., Yurt, R., Himel, H., and Rafii, S. (2001) *Circ. Res.* **88**, 167–174
8. Peichev, M., Naiyer, A. J., Pereira, D., Zhu, Z., Lane, W. J., Williams, M.,

Oz, M. C., Hicklin, D. J., Witte, L., Moore, M. A., and Rafii, S. (2000) *Blood* **95,** 952–958
9. Rehman, J., Li, J., Orschell, C. M., and March, K. L. (2003) *Circulation* **107,** 1164–1169
10. Kocher, A. A., Schuster, M. D., Szabolcs, M. J., Takuma, S., Burkhoff, D., Wang, J., Homma, S., Edwards, N. M., and Itescu, S. (2001) *Nat. Med.* **7,** 430–436
11. Bahlmann, F. H., De Groot, K., Spandau, J. M., Landry, A. L., Hertel, B., Duckert, T., Boehm, S. M., Menne, J., Haller, H., and Fliser, D. (2004) *Blood* **103,** 921–926
12. Bahlmann, F. H., DeGroot, K., Duckert, T., Niemczyk, E., Bahlmann, E., Boehm, S. M., Haller, H., and Fliser, D. (2003) *Kidney Int.* **64,** 1648–1652
13. Heeschen, C., Aicher, A., Lehmann, R., Fichtlscherer, S., Vasa, M., Urbich, C., Mildner-Rihm, C., Martin, H., Zeiher, A. M., and Dimmeler, S. (2003) *Blood* **102,** 1340–1346
14. Dimmeler, S., Aicher, A., Vasa, M., Mildner-Rihm, C., Adler, K., Tiemann, M., Rutten, H., Fichtlscherer, S., Martin, H., and Zeiher, A. M. (2001) *J. Clin. Investig.* **108,** 391–397
15. Llevadot, J., Murasawa, S., Kureishi, Y., Uchida, S., Masuda, H., Kawamoto, A., Walsh, K., Isner, J. M., and Asahara, T. (2001) *J. Clin. Investig.* **108,** 399–405
16. Kaushansky, K., Lok, S., Holly, R. D., Broudy, V. C., Lin, N., Bailey, M. C., Forstrom, J. W., Buddle, M. M., Oort, P. J., Hagen, F. S., Roth, G. J., Papayannopoulou, T., and Foster, D. C. (1994) *Nature* **369,** 568–571
17. Fox, N., Priestley, G., Papayannopoulou, T., and Kaushansky, K. (2002) *J. Clin. Investig.* **110,** 389–394
18. Kimura, S., Roberts, A. W., Metcalf, D., and Alexander, W. S. (1998) *Proc. Natl. Acad. Sci. U. S. A.* **95,** 1195–1200
19. Sitnicka, E., Lin, N., Priestley, G. V., Fox, N., Broudy, V. C., Wolf, N. S., and Kaushansky, K. (1996) *Blood* **87,** 4998–5005
20. Brizzi, M. F., Battaglia, E., Montrucchio, G., Dentelli, P., Del Sorbo, L., Garbarino, G., Pegoraro, L., and Camussi, G. (1999) *Circ. Res.* **84,** 785–796
21. Kaushansky, K., Lin, N., Grossmann, A., Humes, J., Sprugel, K. H., and Broudy, V. C. (1996) *Exp. Hematol.* **24,** 265–269
22. Broudy, V. C., Lin, N. L., and Kaushansky, K. (1995) *Blood* **85,** 1719–1726
23. Kaushansky, K., Broudy, V. C., Grossmann, A., Humes, J., Lin, N., Ren, H. P., Bailey, M. C., Papayannopoulou, T., Forstrom, J. W., and Sprugel, K. H. (1995) *J. Clin. Investig.* **96,** 1683–1687
24. Kobayashi, M., Laver, J. H., Kato, T., Miyazaki, H., and Ogawa, M. (1995) *Blood* **86,** 2494–2499
25. Kanayasu-Toyoda, T., Yamaguchi, T., Oshizawa, T., and Hayakawa, T. (2003) *J. Cell. Physiol.* **195,** 119–129
26. Hur, J., Yoon, C. H., Kim, H. S., Choi, J. H., Kang, H. J., Hwang, K. K., Oh, B. H., Lee, M. M., and Park, Y. B. (2004) *Arterioscler. Thromb. Vasc. Biol.* **24,** 288–293
27. Yoon, C. H., Hur, J., Park, K. W., Kim, J. H., Lee, C. S., Oh, I. Y., Kim, T. Y., Cho, H. J., Kang, H. J., Chae, I. H., Yang, H. K., Oh, B. H., Park, Y. B., and Kim, H. S. (2005) *Circulation* **112,** 1618–1627
28. Miyakawa, Y., Rojnuckarin, P., Habib, T., and Kaushansky, K. (2001) *J. Biol. Chem.* **276,** 2494–2502
29. Drachman, J. G., Sabath, D. F., Fox, N. E., and Kaushansky, K. (1997) *Blood* **89,** 483–492
30. Kirito, K., Watanabe, T., Sawada, K., Endo, H., Ozawa, K., and Komatsu, N. (2002) *J. Biol. Chem.* **277,** 8329–8337
31. Li, A., Dubey, S., Varney, M. L., Dave, B. J., and Singh, R. K. (2003) *J. Immunol.* **170,** 3369–3376
32. Mizukami, Y., Jo, W. S., Duerr, E. M., Gala, M., Li, J., Zhang, X., Zimmer, M. A., Iliopoulos, O., Zukerberg, L. R., Kohgo, Y., Lynch, M. P., Rueda, B. R., and Chung, D. C. (2005) *Nat. Med.* **11,** 992–997
33. Salcedo, R., Ponce, M. L., Young, H. A., Wasserman, K., Ward, J. M., Kleinman, H. K., Oppenheim, J. J., and Murphy, W. J. (2000) *Blood* **96,** 34–40
34. Lin, Y., Weisdorf, D. J., Solovey, A., and Hebbel, R. P. (2000) *J. Clin. Investig.* **105,** 71–77
35. Assmus, B., Schachinger, V., Teupe, C., Britten, M., Lehmann, R., Dobert, N., Grunwald, F., Aicher, A., Urbich, C., Martin, H., Hoelzer, D., Dimmeler, S., and Zeiher, A. M. (2002) *Circulation* **106,** 3009–3017
36. Kalka, C., Masuda, H., Takahashi, T., Kalka-Moll, W. M., Silver, M., Kearney, M., Li, T., Isner, J. M., and Asahara, T. (2000) *Proc. Natl. Acad. Sci. U. S. A.* **97,** 3422–3427
37. Kawamoto, A., Gwon, H. C., Iwaguro, H., Yamaguchi, J. I., Uchida, S., Masuda, H., Silver, M., Ma, H., Kearney, M., Isner, J. M., and Asahara, T. (2001) *Circulation* **103,** 634–637
38. Kirito, K., Fox, N., Komatsu, N., and Kaushansky, K. (2005) *Blood* **105,** 4258–4263
39. Kelemen, E., Cserhati, I., and Tanos, B. (1958) *Acta Haematol. (Basel)* **20,** 350–355
40. Yamamoto, S. (1957) *Acta Haematol. Jpn.* **20,** 163
41. Kanayasu-Toyoda, T., Yamaguchi, T., Uchida, E., and Hayakawa, T. (1999) *J. Biol. Chem.* **274,** 25471–25480
42. Yamaguchi, T., Mukasa, T., Uchida, E., Kanayasu-Toyoda, T., and Hayakawa, T. (1999) *J. Biol. Chem.* **274,** 15575–15581
43. Miyamoto, K., Nishigami, K., Nagaya, N., Akutsu, K., Chiku, M., Kamei, M., Soma, T., Miyata, S., Higashi, M., Tanaka, R., Nakatani, T., Nonogi, H., and Takeshita, S. (2006) *Circulation* **114,** 2679–2684
44. George, J., Afek, A., Abashidze, A., Shmilovich, H., Deutsch, V., Kopolovich, J., Miller, H., and Keren, G. (2005) *Arterioscler. Thromb. Vasc. Biol.* **25,** 2636–2641

THE JOURNAL OF BIOLOGICAL CHEMISTRY VOL. 282, NO. 32, pp. 23117–23128, August 10, 2007

$G\alpha_{12/13}$-mediated Up-regulation of TRPC6 Negatively Regulates Endothelin-1-induced Cardiac Myofibroblast Formation and Collagen Synthesis through Nuclear Factor of Activated T Cells Activation*[S]

Received for publication, December 22, 2007, and in revised form, May 25, 2007 Published, JBC Papers in Press, May 28, 2007, DOI 10.1074/jbc.M611780200

Motohiro Nishida[‡], Naoya Onohara[‡], Yoji Sato[§], Reiko Suda[‡], Mariko Ogushi[‡], Shihori Tanabe[§], Ryuji Inoue[¶], Yasuo Mori[‖], and Hitoshi Kurose[‡1]

From the [‡]Department of Pharmacology and Toxicology, Graduate School of Pharmaceutical Sciences, Kyushu University, 3-1-1 Maidashi, Higashi-ku, Fukuoka 812-8582, [§]National Institute of Health Sciences, Setagaya, Tokyo 158-8501, the [¶]Department of Physiology, School of Medicine, Fukuoka University, Jonan-ku, Fukuoka 814-0180, and the [‖]Laboratory of Molecular Biology, Department of Synthetic Chemistry and Biological Chemistry, Graduate School of Engineering, Kyoto University, Kyoto 615-8510, Japan

Sustained elevation of $[Ca^{2+}]_i$ has been implicated in many cellular events. We previously reported that α subunits of G_{12} family G proteins ($G\alpha_{12/13}$) participate in sustained Ca^{2+} influx required for the activation of nuclear factor of activated T cells (NFAT), a Ca^{2+}-responsive transcriptional factor, in rat neonatal cardiac fibroblasts. Here, we demonstrate that $G\alpha_{12/13}$-mediated up-regulation of canonical transient receptor potential 6 (TRPC6) channels participates in sustained Ca^{2+} influx and NFAT activation by endothelin (ET)-1 treatment. Expression of constitutively active $G\alpha_{12}$ or $G\alpha_{13}$ increased the expression of TRPC6 proteins and basal Ca^{2+} influx activity. The treatment with ET-1 increased TRPC6 protein levels through $G\alpha_{12/13}$, reactive oxygen species, and c-Jun N-terminal kinase (JNK)-dependent pathways. NFAT is activated by sustained increase in $[Ca^{2+}]_i$ through up-regulated TRPC6. A $G\alpha_{12/13}$-inhibitory polypeptide derived from the regulator of the G-protein signaling domain of p115-Rho guanine nucleotide exchange factor and a JNK inhibitor, SP600125, suppressed the ET-1-induced increase in expression of marker proteins of myofibroblast formation through a $G\alpha_{12/13}$-reactive oxygen species-JNK pathway. The ET-1-induced myofibroblast formation was suppressed by overexpression of TRPC6 and CA NFAT, whereas it was enhanced by TRPC6 small interfering RNAs and cyclosporine A. These results suggest two opposite roles of $G\alpha_{12/13}$ in cardiac fibroblasts. First, $G\alpha_{12/13}$ mediate ET-1-induced myofibroblast formation. Second, $G\alpha_{12/13}$ mediate TRPC6 up-regulation and NFAT activation that negatively regulates ET-1-induced myofibroblast formation. Furthermore, TRPC6 mediates hypertrophic responses in cardiac myocytes but suppresses fibrotic responses in cardiac fibroblasts. Thus, TRPC6 mediates opposite responses in cardiac myocytes and fibroblasts.

Structural remodeling of the heart is a key determinant of clinical outcome in heart disease (1–3). Such remodeling involves the overproduction of ECM[2] proteins, predominantly collagen types I and III, into the interstitial and perivascular space. Excessive collagen deposition increases myocardial stiffness and leads to diastolic dysfunction (2–4). Cardiac fibroblasts, constituting 60–70% of total cell numbers in the heart, are responsible for collagen deposition and create the scaffold for cardiac myocytes. Transformation of cardiac fibroblasts to myofibroblasts, characterized by the expression of α-SMA, has been implicated in diseases with increased ECM deposition and resultant cardiac fibrosis (4–6). Myofibroblast formation is controlled by various profibrotic stimuli, such as growth factors, cytokines, and mechanical stretch (5–8). Although several hormones, such as Ang II and ET-1, that stimulate G protein-coupled receptors also induce myofibroblast formation (9, 10), the molecular mechanism is not fully understood.

Sustained elevation of $[Ca^{2+}]_i$, induced by increased Ca^{2+} influx, is important for the regulation of diverse cellular processes, such as gene expression, cell proliferation, and differentiation.

* This work was supported by grants from the Ministry of Education, Culture, Sports, Science, and Technology of Japan (to M. N. and H. K.); from the Ministry of Health, Labour, and Welfare of Japan and the National Institute of Biomedical Innovation (MF-16) (to Y. S.); from the Program for Promotion of Fundamental Studies in Health Sciences of the National Institute of Biomedical Innovation (NIBIO), the Naito Foundation, and Takeda Science Foundation (to M. N.); and from the Astellas Foundation for Research on Metabolic Disorders and the Kimura Memorial Heart Foundation Research Grant for 2006 (to H. K.). The costs of publication of this article were defrayed in part by the payment of page charges. This article must therefore be hereby marked "*advertisement*" in accordance with 18 U.S.C. Section 1734 solely to indicate this fact.

[S] The on-line version of this article (available at http://www.jbc.org) contains supplemental Figs. 1 and 2.

[1] To whom correspondence should be addressed. Tel./Fax: 81-92-642-6884; E-mail: kurose@phar.kyushu-u.ac.jp.

[2] The abbreviations used are: ECM, extracellular matrix; Ang, angiotensin; CA, constitutively active; CysA, cyclosporine A; DAG, diacylglycerol; DN, dominant negative; DPI, diphenyleneiodonium; EGFR, epidermal growth factor receptor; ET-1, endothelin-1; GFP, green fluorescent protein; JNK, c-Jun NH_2-terminal kinase; NFAT, nuclear factor of activated T cells; p115-RGS, RGS domain of p115Rho guanine nucleotide exchange factor; PLC, phospholipase C; RACC, receptor-activated Ca^{2+} channel; RGS, regulator of G-protein signaling; ROS, reactive oxygen species; RT, reverse transcription; siRNA, small interfering RNA; α-SMA, α-smooth muscle actin; SOCs, store-operated Ca^{2+} channels; TRPC, canonical transient receptor potential; WT, wild type; ERK, extracellular signal-regulated kinase; PP2, 4-amino-5-(4-chlorophenyl)-7-(*t*-butyl)pyrazolo[3,4-*d*]pyrimidine; OAG, a DAG derivative, 1-oleoyl-2-acyl-sn-glycerol.

In the heart, a Ca^{2+}-responsive serine/threonine phosphatase calcineurin is activated by sustained $[Ca^{2+}]_i$ increase, and calcineurin activation has been implicated in hypertrophic growth of cardiomyocytes (11, 12). Activated calcineurin dephosphorylates the transcriptional factor NFAT, facilitating translocation of NFAT from cytosol to the nucleus, where it acts synergistically with other partners to mediate the expression of prohypertrophic genes. However, the physiological and pathological roles of calcineurin-NFAT signaling in cardiac fibroblasts are still controversial when the roles of the signaling pathway are analyzed by CysA, a calcineurin inhibitor. It has been reported that treatment with CysA inhibits pressure overload-induced cardiac hypertrophy and fibrosis (13) and enhances cardiac dysfunction during postinfarction failure (14). Other reports have demonstrated that myocardial fibrosis is promoted in transplanted hearts (15) or chronically aortic banded hearts (16) treated with CysA. Cardiac fibrosis *in vivo* often follows the development of cardiac hypertrophy. To understand fibrotic pathways, it is essential to examine mechanisms of cardiac fibrosis and hypertrophy individually. Although the role of NFAT in cardiac hypertrophy is established, the role of NFAT in cardiac fibrosis is still unknown.

We previously reported that $G\alpha_{12/13}$ mediate Ang II-induced NFAT activation in cardiac fibroblasts (17). We also demonstrated that activation of $G\alpha_{13}$ increases basal Ca^{2+} influx activity, which is completely suppressed by SK&F96365, an inhibitor of RACCs (18). Members of the TRPC family channels are thought to be molecular candidates for RACCs (19). Recent reports have implicated the involvement of TRPC up-regulation in diseases with abnormal Ca^{2+} handling and resultant heart failure (20, 21). We recently reported that TRPC3 and TRPC6 are involved in Ang II-induced hypertrophic responses of rat neonatal cardiomyocytes (12). However, it is still unknown whether TRPC channels participate in $G\alpha_{12/13}$-mediated NFAT activation and agonist-induced myofibroblast formation in cardiac fibroblasts.

In this study, we investigate how the expression of TRPC channels is regulated and whether TRPC channels are involved in the $G\alpha_{12/13}$-mediated increase in basal Ca^{2+} influx required for NFAT activation. We also examine the roles of TRPC channels and NFAT in transformation of cardiac fibroblasts to myofibroblasts.

EXPERIMENTAL PROCEDURES

Materials and Plasmid Construction—JNK inhibitor II (SP600125), cyclosporine A, and PP2 were purchased from Calbiochem. Ang II, ET-1, DPI, U73122, Igepal CA-630, BQ123, BQ788, and anti-α-SMA antibody (clone 1A4) were purchased from Sigma. Fura-2/AM was from Dojindo (Kumamoto, Japan). Collagenase and Fugene 6 were from Roche Applied Science. Dual luciferase reagents was from Promega. pNFAT-Luc and pRL-SV40 vectors were from Stratagene. Anti-TRPC3 and anti-TRPC6 antibodies were from Alomone Laboratories. Anti-TRPC7 antibody was prepared by Y. Mori. Anti-phospho-ERK, anti-ERK, anti-phospho-Src (Tyr^{416}), and anti-Src antibodies were from Cell Signaling. Anti-glyceraldehyde-3-phosphate dehydrogenase, anti-JNK1, horseradish peroxidase-conjugated anti-rabbit IgG, and anti-mouse IgG antibodies were from Santa Cruz Biotechnology, Inc. (Santa Cruz, CA). Anti-Rac antibody was from Transduction Laboratories. CA NFAT was first inserted into the pEGFP-C1 vector (Clontech) and transferred into pShuttle-cytomegalovirus vector to produce recombinant adenovirus. A 913-bp fragment containing the upstream region and the 5′-untranslated region of the rat TRPC6 gene[3] was isolated by PCR using rat genomic DNA as a template, and the fragment was inserted upstream of a luciferase gene in the pGL3-Basic vector using KpnI/BglII sites.

Cell Culture—Cardiac fibroblasts and myocytes were prepared from ventricles of 1–2-day-old Sprague-Dawley rats (17, 22). Briefly, after digestion of ventricles with 0.1% collagenase, isolated fibroblasts were plated on a noncoated dish in Dulbecco's modified Eagle's medium containing 10% fetal bovine serum and 50 units/ml penicillin/streptomycin. Subconfluent cells were serum-starved for 48 h and used for the experiments. Considering the possibility that cardiac fibroblasts may lose the original characteristics after prolonged culture, cells were used within two passages in all experiments.

Production of Adenoviruses, Infection, and Transfection—Recombinant adenoviruses used in this study, including WT TRPC6, DN TRPC6 (C6-3A and C6-ΔN), GFP-fused N-terminal region of NFAT4 (GFP-NFAT4), and CA NFAT, were produced as described previously (12, 23–25). Cells were infected with adenovirus(es) at a multiplicity of infection of 100 for 48 h. Small interference RNAs (100 nM) were transfected with Lipofectamine 2000 for 72 h.

Measurement of Intracellular Ca^{2+} Measurement and NFAT Activity—The intracellular Ca^{2+} concentration ($[Ca^{2+}]_i$) of cardiac fibroblasts was determined by a method described previously (17). Fluorescence images of GFP-positive cells were recorded and analyzed with a video image analysis system (Aquacosmos, Hamamatsu Photonics). Measurement of NFAT activity was performed as described previously (17). For measuring the translocation of GFP-NFAT4, cells (1.5×10^5) plated on glass bottom 35-mm dishes were infected for 48 h with adenovirus coding GFP-NFAT4 at a multiplicity of infection of 30. After ET-1 stimulation (100 nM) for 48 h, the localization of GFP-NFAT4 was determined with a laser-scanning confocal imaging system (LSM510; Carl Zeiss).

Measurement of ROS Production—Measurement of intracellular ROS concentration was performed in 2 mM Ca^{2+}-containing Hepes-buffered saline solution (107 mM NaCl, 6 mM KCl, 11.5 mM glucose, 20 mM HEPES, pH 7.4, 1.2 mM $MgSO_4$, 2 mM $CaCl_2$) with a fluorescent dye, 2′,7′-dichlorofluorescein diacetate as described previously (17). Fluorescence images were recorded and analyzed with a video image analysis system (Aquacosmos, Hamamatsu Photonics). The peak changes ($\Delta F/F_0$) of DCF fluorescence intensity were identified as values obtained by subtracting the basal fluorescence intensity (F_0) from the maximal intensity during 5-min ET-1 treatment.

Expression Analysis of TRPC mRNAs—The RT-PCR protocol used for the expression analysis and the PCR primers used in this study were as described previously (26). Real time RT-PCR for quantitative measurement was performed as described pre-

[3] The sequence was obtained from Ref. 37 (GenBank™ accession number NW_047798).

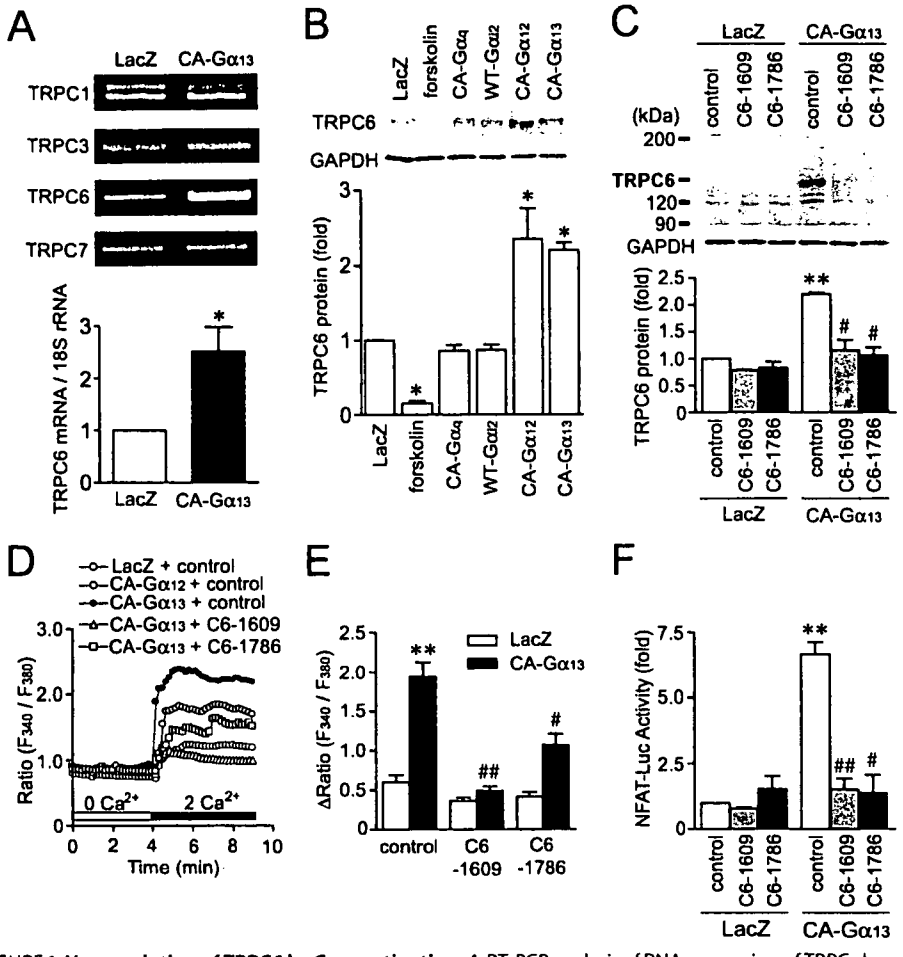

FIGURE 1. **Up-regulation of TRPC6 by $G\alpha_{13}$ activation.** *A*, RT-PCR analysis of RNA expression of TRPC channels in LacZ- and CA $G\alpha_{13}$-expressing cardiac fibroblasts. *Bottom*, real time RT-PCR analysis of RNA expression of TRPC6. *B*, expression of TRPC6 protein in LacZ-expressing and the respective Gα-overexpressing cells. Cells were treated with forskolin (50 μM) for 24 h. *C*, effects of TRPC6 siRNAs (C6-1609 and C6-1786) on TRPC6 protein expression. *D*, effects of TRPC6 siRNAs on the basal Ca^{2+} influx activity in CA $G\alpha_{13}$-expressing cells. Four min after Ca^{2+} measurement in Ca^{2+}-free solution, basal Ca^{2+} influx was determined by the addition of 2 mM Ca^{2+}. *E*, the amplitude of maximum $[Ca^{2+}]_i$ rises (ΔRatio) induced by the addition of 2 mM Ca^{2+} was calculated. *F*, effects of TRPC6 siRNAs on CA $G\alpha_{13}$-induced increase in NFAT activity. *, $p < 0.05$; **, $p < 0.01$ *versus* control of LacZ-expressing cells. #, $p < 0.05$; ##, $p < 0.01$ *versus* control of CA $G\alpha_{13}$-expressing cells.

viously (18). Briefly, total RNA (150 ng) was subjected to real time RT-PCR. Oligonucleotide primers and fluorescence-labeled TaqMan® probes were designed with Primer Express software (Applied Biosystems, Foster City, CA). Primers and probe were as follows: for rat TRPC6 mRNA, forward primer (5′-AGCAGCAGCTCCTCTCCATATG-3′), reverse primer (5′-GAGGACCACGAGGAATTTCACT-3′), and TaqMan® probe (5′-TATGAGAACCTCTCTGGTTTACGGCAGCA-3′); for collagen type I, forward primer (5′-GGAGAGTACTGGATCGACCCTAAC-3′), reverse primer (5′-CTGACCTGTCTCCATGTTGCA-3′), and TaqMan® probe (5′-AAGGCTGCAACCTGGATGCCATCAA-3′); for collagen type III, forward primer (5′-CCTGCTTCACCCCTCTCTTATTT-3′), reverse primer (5′-TCCCGAGTCGCAGACACATAT-3′), and TaqMan® probe (5′-TAGAGATGTCTGGAAGCCAGAACCATGTCA-3′). All reactions were performed in TaqMan® One-Step RT-PCR Master Mix Reagents (Applied Biosystems) and the Applied Biosystems 7500 real time PCR system. The rat glyceraldehyde-3-phosphate dehydrogenase mRNA (Applied Biosystems (catalog number 4308313)) was used as an internal control to normalize the differences in the amount of total RNA in each sample.

Western Blot Analysis—Cardiac fibroblasts (3×10^5 cells) plated on 6-well dishes were directly harvested with 200 μl of 2× SDS sample buffer. The protein samples (20 μl) were fractionated by 8% SDS-polyacrylamide gel and then transferred onto polyvinylidene difluoride membrane. The expression of endogenous TRPC proteins was assessed by Western blotting using anti-TRPC antibodies (12, 27). The Src and ERK activities were assessed by using anti-phospho-specific antibodies. The JNK activity was assessed as described previously (23–25). For α-SMA expression, cells were harvested with lysis buffer containing 50 mM Tris-HCl (pH 7.5), 150 mM NaCl, 1% Igepal CA-630, and protease inhibitor mixture (6). The protein samples were fractionated by 10% SDS-PAGE.

Measurement of Rac Activity—Activation of small G proteins was determined by the method of Nishida *et al.* (25). Activated Rac was pulled down with 10 μg of glutathione *S*-transferase-fused Rac-interacting domain of p21-activated kinase (PAK-CRIB). Pulled down small G proteins were detected with anti-Rac1 antibody.

Measurement of Cardiac Myofibroblast Formation—Transformation of cardiac fibroblasts to myofibroblasts was assessed by the expression of α-SMA and production of ECM components (6). Briefly, 24 h after infection, cardiomyocytes were stimulated with ET-1 (100 nM) for 48 h. The cells were washed, fixed, incubated with anti-α-SMA antibody, and then stained with Alexa Fluor 546 goat anti-mouse IgG. Morphological changes and α-SMA expression of cardiac fibroblasts were visualized with confocal microscopy. For the measurement of collagen synthesis, cells were harvested with lysis buffer containing 50 mM Tris-HCl (pH 7.5), 150 mM NaCl, 1% Igepal CA-630, and protease inhibitor mixture (Nacalai, Japan). Production of ECM components was assessed by [^{3}H]proline incorporation. After cells were stimulated with ET-1 (100 nM) for 2 h, [^{3}H]proline (1 μCi/ml) was added to the culture medium and further incubated for 6 h. The incorporated [^{3}H]proline was extracted by 1 N NaOH overnight and measured using a liquid scintillation counter.

Measurement of Hypertrophic Responses of Cardiomyocytes—Preparation of rat neonatal cardiomyocytes and measurement of hypertrophic responses were performed as described (12).

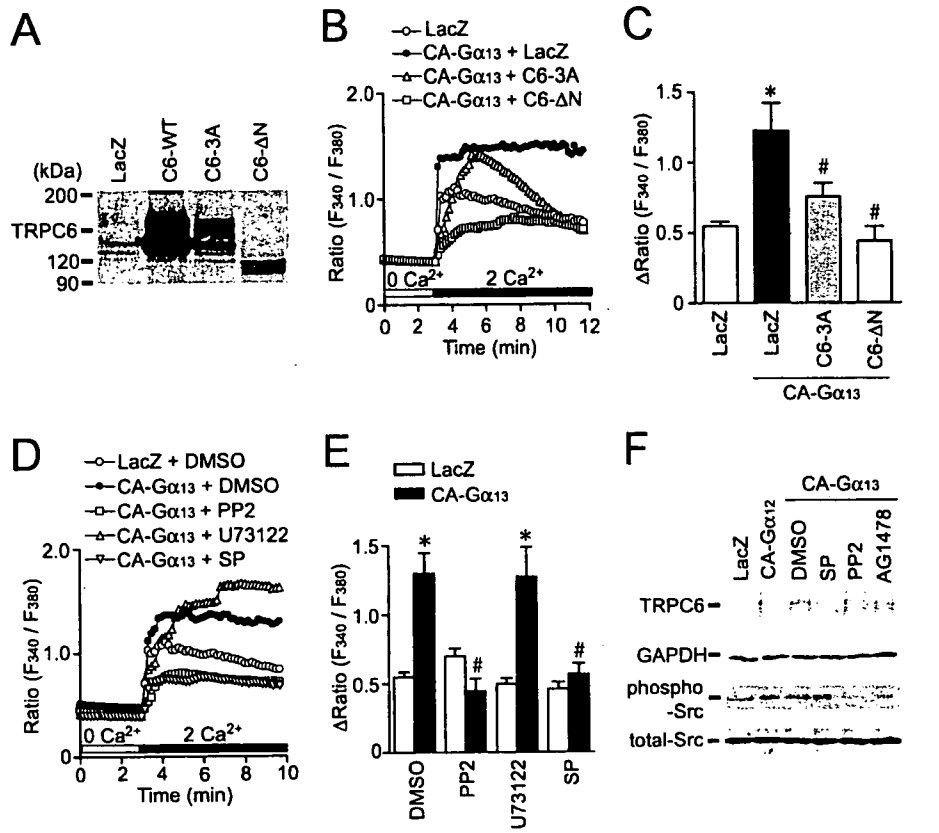

FIGURE 2. **Involvement of tyrosine kinase in CA $G\alpha_{13}$-induced increase in basal Ca^{2+} influx activity in cardiac fibroblasts.** *A*, expression of wild type TRPC6 (*WT*) and DN TRPC6 (C6-3A and C6-ΔN) proteins in cardiac fibroblasts. One-fourth volume of protein samples (5 μl) was subjected to 7% SDS-PAGE. The expression level of endogenous TRPC6 was low, and expression levels of wild type and mutated TRPC6 were very high. Therefore, the band intensity of endogenous TRPC6 is weak under these conditions. *B* and *C*, effects of DN TRPC6 proteins on the CA $G\alpha_{13}$-induced increase in basal Ca^{2+} influx activity. *B*, average time courses of Ca^{2+} responses induced by the addition of 2 mM Ca^{2+}. *C*, the amplitude of sustained $[Ca^{2+}]_i$ increase 4 min after the addition of 2 mM Ca^{2+}. *D* and *E*, effects of PP2, SP600125 (*SP*), and U73122 on the CA $G\alpha_{13}$-induced increase in basal Ca^{2+} influx activity. Cells were treated with PP2 (1 μM) or U73122 (1 μM) for 20 min and SP600125 (1 μM) for 48 h prior to $[Ca^{2+}]_i$ measurement. *D*, average time courses of Ca^{2+} responses. *E*, peak changes in $[Ca^{2+}]_i$ induced by the addition of 2 mM Ca^{2+}. *F*, effects of SP600125, PP2, and AG1478 on CA $G\alpha_{13}$-induced increase in TRPC6 protein expression and Src phosphorylation. Cells were treated with SP600125 (1 μM) for 48 h and with PP2 (1 μM) or AG1478 (1 μM) for 30 min prior to cell harvest. *, $p < 0.05$ *versus* LacZ-expressing cells. #, $p < 0.05$ *versus* control (LacZ or Me_2SO (*DMSO*)) of CA $G\alpha_{13}$-expressing cells.

Briefly, 48 h after siRNA treatment, cardiomyocytes were stimulated with ET-1 (100 nM) for 24 h. The cells were stained with Alexa Fluor 594-phalloidin to visualize actin filament. Protein synthesis was measured by [^{3}H]leucine incorporation. After cells were stimulated with ET-1 (100 nM) for 2 h, [^{3}H]leucine (1 μCi/ml) was added and further incubated for 6 h.

Statistical Analysis—The results are presented as mean ± S.E. The data were accumulated under each condition from at least three independent experiments. For the measurements of $[Ca^{2+}]_i$, representative data of time course experiments were plotted from one of three similar experiments that were performed with more than 30 cells. Mean values were compared with control by Student's *t* test.

RESULTS

Up-regulation of TRPC6 Proteins by $G\alpha_{13}$ Activation—We previously demonstrated that the expression of GTPase-defective mutants of $G\alpha_{12}$ (Q229L; CA $G\alpha_{12}$) and $G\alpha_{13}$ (Q226L; CA $G\alpha_{13}$) increases $[Ca^{2+}]_i$ and NFAT activity through an SK&F96365-sensitve Ca^{2+} influx pathway (17, 18). TRPC channels are thought to be molecular candidates for RACCs. Thus, we examined which TRPC channels are expressed in rat cardiac fibroblasts. Among TRPC1 to -7 channels, TRPC1, TRPC3, TRPC6, and TRPC7 mRNAs were detected (Fig. 1*A*). Interestingly, only TRPC6 mRNA expression was increased 2.5-fold by the expression of CA $G\alpha_{13}$. The expression of TRPC6 proteins was also increased by CA $G\alpha_{12}$ (Fig. 1*B*). Expression of CA $G\alpha_q$ (R183C) and WT $G\alpha_{i2}$ did not increase TRPC6 protein levels, although both mutants significantly increased ERK activity (supplemental Fig. 1). Treatment with forskolin (50 μM) rather decreased basal expression of TRPC6 proteins. These results indicate that $G\alpha_{12/13}$ specifically up-regulate TRPC6 proteins in cardiac fibroblasts. In order to examine whether up-regulation of TRPC6 participates in CA $G\alpha_{12/13}$-induced enhancement of Ca^{2+} responses, knockdown experiments of TRPC6 proteins were performed by using TRPC6 siRNAs (12). Since the extent of NFAT activation induced by CA $G\alpha_{13}$ was larger than that by CA $G\alpha_{12}$, CA $G\alpha_{13}$-expressing cells were used to examine the involvement of TRPC6 in $G\alpha_{12/13}$-mediated Ca^{2+} responses. Treatment with TRPC6 siRNAs completely suppressed CA $G\alpha_{13}$-induced up-regulation of TRPC6 protein expression (Fig. 1*C*). We confirmed that TRPC6 siRNAs did not affect the expression levels of TRPC3 and TRPC7 proteins (data not shown). The basal Ca^{2+} influx activity was determined by the increase in $[Ca^{2+}]_i$ induced by the addition of 2 mM extracellular Ca^{2+} to cells in Ca^{2+}-free Tyrode's solution (18). This basal Ca^{2+} influx activity was enhanced by the expression of CA $G\alpha_{13}$ and CA $G\alpha_{12}$ (Fig. 1*D*). The CA $G\alpha_{13}$-induced increase in $[Ca^{2+}]_i$ was completely suppressed by the treatment with TRPC6 siRNAs (Fig. 1, *C–E*). The sustained increase in $[Ca^{2+}]_i$ activated NFAT activity, and the treatment with TRPC6 siRNAs inhibited CA $G\alpha_{13}$-induced NFAT activation (Fig. 1*F*). These results suggest that up-regulation of TRPC6 by $G\alpha_{13}$ activation enhances Ca^{2+} influx and NFAT activation in cardiac fibroblasts.

Involvement of Tyrosine Kinase in TRPC6-mediated Ca^{2+} Influx by $G\alpha_{12/13}$ Activation—We next examined whether the channel activity of TRPC6 proteins is actually enhanced by $G\alpha_{13}$ activation. WT TRPC6 or two DN mutants of TRPC6 (C6-3A and C6-ΔN) were overexpressed in cardiac fibroblasts (Fig. 2*A*). The expression of DN TRPC6 significantly sup-

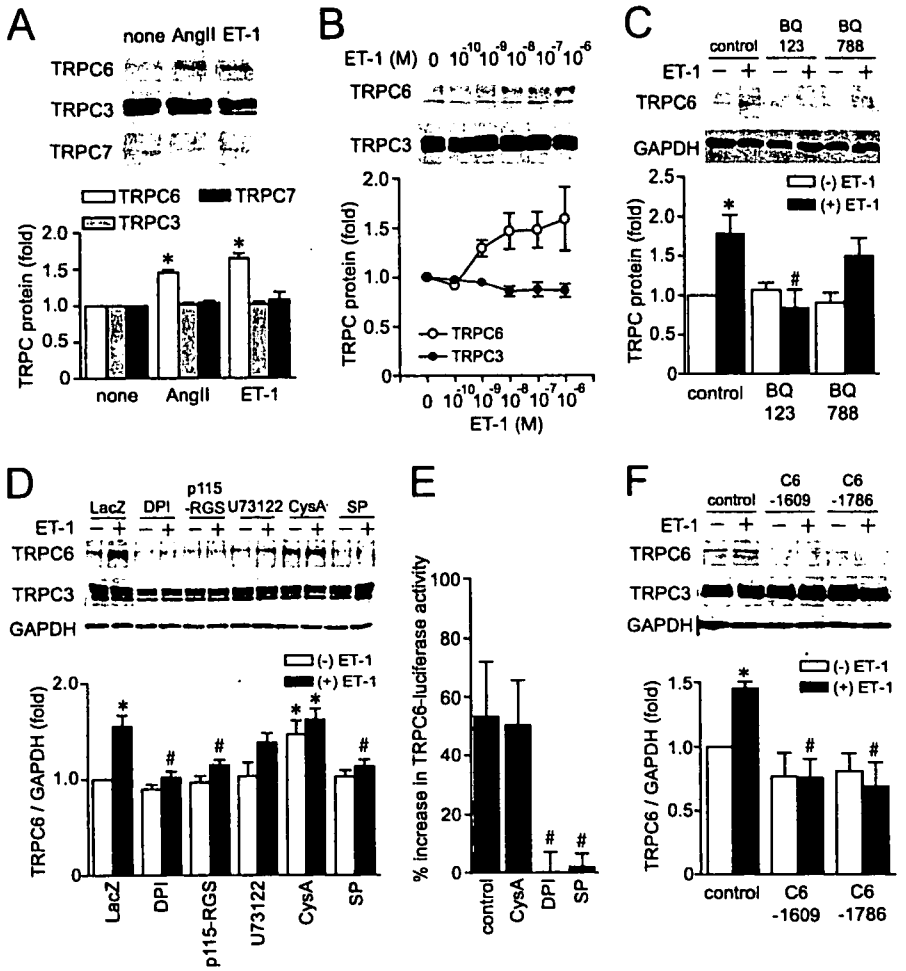

FIGURE 3. **ET-1 up-regulates TRPC6 through the $G\alpha_{13}$-ROS-JNK-dependent pathway.** *A*, changes in expression levels of TRPC3, TRPC6, and TRPC7 proteins by the treatment with Ang II (100 nM) and ET-1 (100 nM) for 48 h. *B*, concentration-dependent increase in TRPC6 protein expression by ET-1 treatment. *C*, effects of ET receptor antagonists on ET-1-induced increase in TRPC6 expression. Cells were treated with BQ123 (3 μM) or BQ788 (3 μM) for 5 min prior to ET-1 stimulation. *D*, involvement of $G\alpha_{12/13}$, ROS, and JNK in the ET-1-induced increase in TRPC6 expression. Twenty-four h after infection with LacZ or p115-RGS, cells were treated with ET-1 (100 nM) for 48 h. Cells were treated with DPI (1 μM), U73122 (1 μM), CysA (0.5 μg/ml), and SP600125 (*SP*; 1 μM) for 20 min prior to ET-1 stimulation. *E*, effects of CysA, DPI, and SP600125 on ET-1-induced increase in the TRPC6-luciferase activity. Cells were treated with ET-1 (100 nM) for 6 h. *F*, effects of TRPC6 siRNAs on TRPC3 and TRPC6 protein expressions. *, $p < 0.05$ *versus* nontreatment (no ET-1) of control or LacZ-expressing cells. #, $p < 0.05$ *versus* ET-1 treatment of control or LacZ-expressing cells.

pressed the sustained $[Ca^{2+}]_i$ increase of CA $G\alpha_{13}$-expressing cells induced by the addition of 2 mM extracellular Ca^{2+} (Fig. 2, *B* and *C*), indicating that the increase in $[Ca^{2+}]_i$ of CA $G\alpha_{13}$-expressing cells is enhanced by Ca^{2+} influx through TRPC6 channels. It has been reported that TRPC6 activity is regulated by DAG (28) and tyrosine phosphorylation (29), and activated $G\alpha_{13}$ induces activation of tyrosine kinase (30, 31) and PLC (32). We examined the involvement of TRPC6 in CA $G\alpha_{13}$-induced $[Ca^{2+}]_i$ increase by determining the requirement of tyrosine phosphorylation or PLC for TRPC6 activation. Treatment with PP2, a Src tyrosine kinase inhibitor, and SP600125, a JNK inhibitor, but not U73122, a PLC inhibitor, significantly suppressed the increase in $[Ca^{2+}]_i$ of CA $G\alpha_{13}$-expressing cells induced by the addition of 2 mM Ca^{2+} (Fig. 2, *D* and *E*). Consistent with the involvement of Src, the expression of CA $G\alpha_{12}$ and CA $G\alpha_{13}$ increased Src activity about 2.5-fold (Fig. 2*F*). CA $G\alpha_{13}$-induced Src activation was suppressed by treatment with AG1478, an EGFR kinase inhibitor (Fig. 2*F*), suggesting that EGFR kinase mediates the CA $G\alpha_{13}$-induced Src activation. Treatment with SP600125, but not PP2 and AG1478, suppressed CA $G\alpha_{13}$-induced up-regulation of TRPC6 protein, whereas treatment with PP2 and AG1478, but not SP600125, suppressed CA $G\alpha_{13}$-induced Src activation (Fig. 2*F*). These results suggest that EGFR- and PP2-sensitive tyrosine kinase(s) participate in $G\alpha_{13}$-mediated enhancement of Ca^{2+} influx independently of TRPC6 up-regulation. These findings are consistent with the report that EGFR participates in $G\alpha_{13}$-mediated responses (33).

Up-regulation of TRPC6 Proteins by ET-1 and Ang II Stimulation—We next examined whether up-regulation of TRPC6 is actually induced by G_{13}-coupled receptor stimulation. We have previously demonstrated that $G\alpha_{12/13}$ mediate Ang II- and ET-1-induced activation of JNK and hypertrophic responses in rat neonatal cardiomyocytes (24, 25). The TRPC6 protein expression levels were significantly increased by Ang II treatment and more potently by ET-1 treatment, in a concentration-dependent manner (Fig. 3, *A* and *B*). Treatment with ET-1 actually increased TRPC6 mRNA levels (supplemental Fig. 2*A*). The up-regulation of TRPC6 protein was detected at 6 h after ET-1 stimulation and the expression of TRPC6 proteins reached a peak at 48 h (data not shown). In contrast to TRPC6, Ang II and ET-1 treatment did not affect the expression levels of TRPC3 and TRPC7 proteins (Fig. 3*A*). These results indicate that ET-1 treatment selectively up-regulates TRPC6 proteins in cardiac fibroblasts. Since the ET-1-induced increase in TRPC6 protein expression levels was completely suppressed by BQ123, a selective ET_A receptor antagonist, but not by BQ788, a selective ET_B receptor antagonist (Fig. 3*C*), the ET_A receptor predominantly mediates ET-1-induced TRPC6 up-regulation. It has been reported that the activation of JNK and STAT3 is required for up-regulation of TRPC6 proteins induced by ET-1 and PDGF stimulation in pulmonary vascular smooth muscle cells (34, 35). We previously demonstrated that $G\alpha_{12/13}$ mediate Ang II-induced Rac activation, ROS production, and JNK activation in cardiac myocytes and fibroblasts (17, 25). Thus, we examined whether ROS and JNK are involved in ET-1-induced TRPC6 up-regulation. Expression of p115-RGS, a selective inhibitory polypeptide of $G\alpha_{12/13}$, completely suppressed ET-1-induced increase in

TRPC6 proteins, as expected (Fig. 3*D*). The ET-1-induced TRPC6 up-regulation was also suppressed by DPI and SP600125 but not by a PLC inhibitor, U73122, and CysA. Since DPI is a selective inhibitor of ROS production by NADPH oxidase complex and SP600125 selectively inhibits JNK activation, these results suggest that the $G\alpha_{12/13}$-ROS-JNK pathway participates in ET-1-induced TRPC6 up-regulation. NFAT is activated through its dephosphorylation by calcineurin that is inhibited by CysA. Since the treatment with CysA increased TRPC6 mRNA levels and the expression of CA NFAT decreased TRPC6 mRNA levels (supplemental Fig. 2*B*), NFAT may negatively regulate ET-1-induced TRPC6 expression in cardiac fibroblasts. Furthermore, the ET-1-induced increase in TRPC6 promoter-dependent luciferase activity was completely suppressed by DPI and SP600125 but not by CysA (Fig. 3*E*). These results suggest that the $G\alpha_{12/13}$-ROS-JNK pathway participates in the transcriptional activation of the TRPC6 gene. ET-1-stimulated up-regulation of TRPC6 protein was completely suppressed by siRNAs against TRPC6 (Fig. 3*F*), suggesting the utility of these siRNAs for future analysis.

Up-regulation of TRPC6 Enhances Receptor-activated Ca^{2+} Responses but Not Store-operated Ca^{2+} Responses—TRPC proteins have been emerged as a candidate subunit of RACCs and SOCs (19). To examine whether up-regulation of TRPC6 enhances receptor-activated or store-operated Ca^{2+} entry, we have individually determined store-operated and receptor-activated Ca^{2+} entry. The increase in $[Ca^{2+}]_i$ through receptor-activated Ca^{2+} entry is determined by the addition of Ca^{2+} after receptor stimulation in the absence of extracellular Ca^{2+}. The increase in $[Ca^{2+}]_i$ through store-operated Ca^{2+} entry is determined by the addition of Ca^{2+} after the treatment of cells with Ca^{2+} ionophore ionomycin in the absence of extracellular Ca^{2+}. Since the cells were treated with ET-1 for long period of time, we used Ang II as a receptor stimulant to avoid the underestimation of ET-1-stimulated increase in $[Ca^{2+}]_i$ through receptor-activated Ca^{2+} entry due to desensitization. The expression of TRPC6 did not affect the Ang II-induced increase in $[Ca^{2+}]_i$ in the absence of extracellular Ca^{2+} but enhanced the increase in $[Ca^{2+}]_i$ by the addition of extracellular Ca^{2+} (Fig. 4, *A* and *B*). The treatment with TRPC6 siRNA (C6-1609) did not affect the initial increase in $[Ca^{2+}]_i$ of ET-1-treated cells (Fig. 4, *A* and *B*). However, TRPC6 siRNA (C6-1609) completely inhibited the increase in $[Ca^{2+}]_i$ induced by the addition of Ca^{2+}. These results are consistent with the findings that the prolonged treatment of cells with ET-1 increases TRPC6 expression. It has been known that TRPC6-mediated Ca^{2+} influx is enhanced by DAG derivative OAG (19). We examined whether OAG-stimulated increases in $[Ca^{2+}]_i$ are suppressed by TRPC6 siRNA. Stimulation with OAG enhanced the increase in $[Ca^{2+}]_i$ induced by the addition of extracellular Ca^{2+} of WT TRPC6-expressing or ET-1-treated cells (Fig. 4, *C* and *D*). TRPC6 siRNA (C6-1609) completely suppressed the OAG-induced increase in $[Ca^{2+}]_i$ of WT TRPC6-expressing or ET-1-treated cells. Although compensatory up-regulation of TRPC3 mRNA expression is reported in TRPC6-deficient mice (36), TRPC6 siRNAs did not affect TRPC3 protein expression (Fig. 3*F*). These results suggest that up-regulation of TRPC6 enhances receptor-activated Ca^{2+} entry through a DAG-dependent mechanism. In contrast to the involvement of TRPC6 in receptor-activated Ca^{2+} entry, overexpression of TRPC6 did not affect Ca^{2+} entry-dependent increase in $[Ca^{2+}]_i$ induced by ionomycin treatment that completely depletes intracellular Ca^{2+} stores (27) (Fig. 4, *E* and *F*). Up-regulation of TRPC6 by ET-1 treatment did not affect the increase in $[Ca^{2+}]_i$ induced by Ca^{2+} entry after ionomycin treatment. These results suggest that the increased expression of TRPC6 does not contribute to the increase in $[Ca^{2+}]_i$ through SOC-mediated Ca^{2+} entry in cardiac fibroblasts. Since the Ang II-induced Ca^{2+} release and

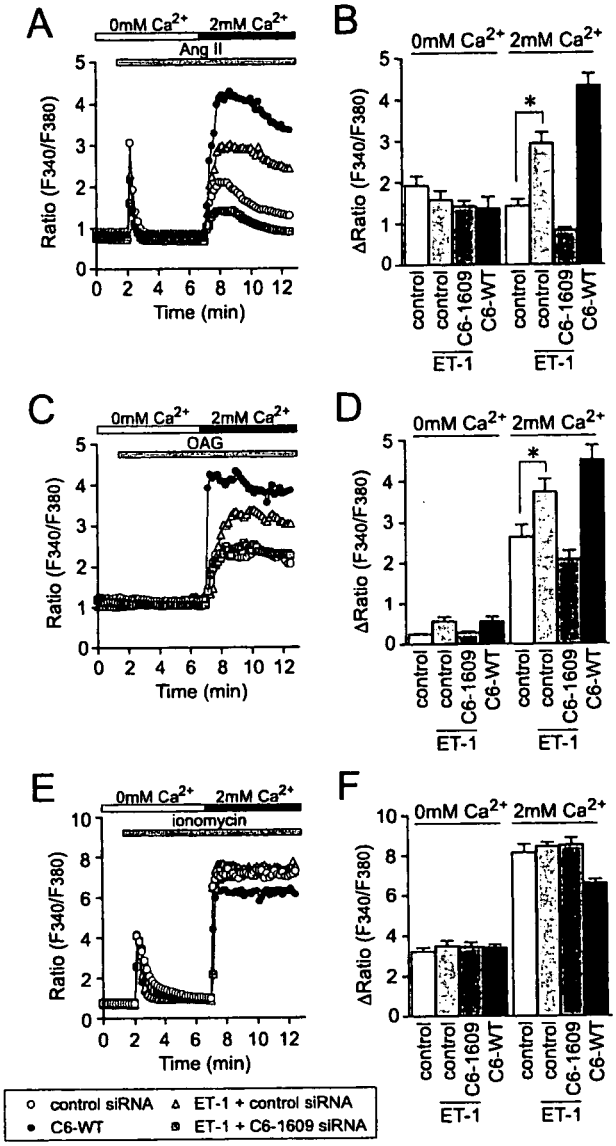

FIGURE 4. **Up-regulation of TRPC6 enhances Ca^{2+} responses induced by Ca^{2+} entry upon receptor stimulation.** *A*, average time courses of Ca^{2+} responses upon Ang receptor stimulation with Ang II (100 nM). Ca^{2+} release was first evoked in Ca^{2+}-free solution, and Ca^{2+} entry-mediated Ca^{2+} responses were induced by the addition of 2 mM Ca^{2+}. Forty-eight h after the transfection with siRNA (control or C6-1609), cells were treated with ET-1 (100 nM) for 48 h, and then $[Ca^{2+}]_i$ levels were measured. *B*, peak Ang II-induced increase in $[Ca^{2+}]_i$ in Ca^{2+}-free solution and after the addition of Ca^{2+}. *C*, average time courses of Ca^{2+} responses induced by OAG (25 μM). *D*, peak OAG-induced $[Ca^{2+}]_i$ increase observed after the addition of Ca^{2+} to Ca^{2+}-free solution. *E*, average time courses of Ca^{2+} responses induced by ionomycin (1 μM). *F*, peak ionomycin-induced $[Ca^{2+}]_i$ increase observed after the addition of Ca^{2+} to Ca^{2+}-free solution. *, $p < 0.05$ *versus* nontreatment (no ET-1) of control cells.

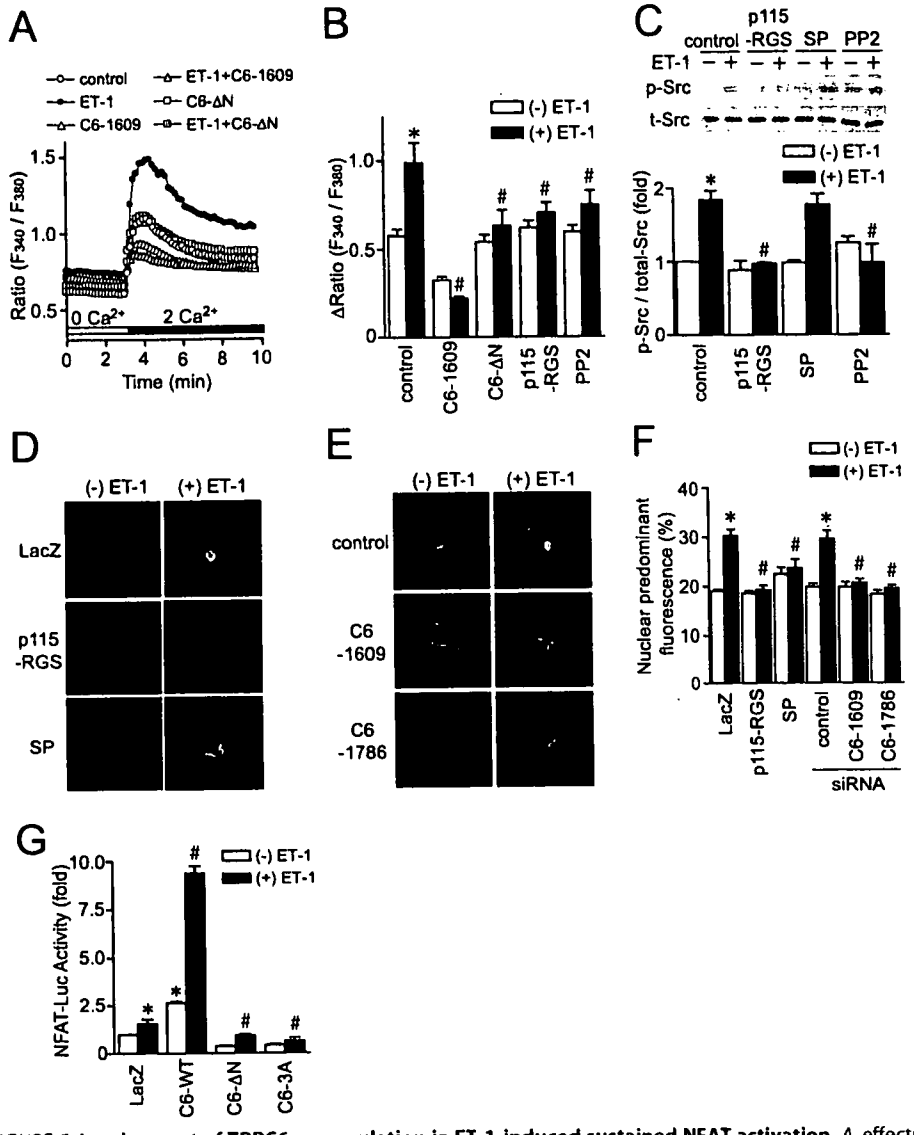

FIGURE 5. **Involvement of TRPC6 up-regulation in ET-1-induced sustained NFAT activation.** *A*, effects of TRPC6 siRNA and DN TRPC6 (C6-ΔN) on the basal Ca^{2+} influx activity in ET-1-treated cells. Twenty-four h after the infection with adenovirus coding C6-ΔN or the transfection with siRNA (C6-1609), cells were treated with ET-1 (100 nM) for 48 h, and then basal Ca^{2+} influx activity was determined. *B*, peak amplitudes of $[Ca^{2+}]_i$ increase, induced by the addition of 2 mM Ca^{2+}. Cells were first treated with ET-1 for 48 h and then treated with SP600125 (*SP*; 1 μM) or PP2 (1 μM) for 20 min prior to $[Ca^{2+}]_i$ measurement. *C*, effects of p115-RGS, PP2, and SP600125 on ET-1-induced Src phosphorylation. Cells were first treated with PP2 and SP600125 for 20 min and then treated with ET-1 for 10 min. *D*, effects of p115-RGS and SP600125 on ET-1-induced nuclear localization of GFP-NFAT4 proteins. *E*, effects of TRPC6 siRNAs on ET-1-induced NFAT translocation. Twenty-four h after the transfection with siRNAs, cells were treated with ET-1 for 48 h, and the localization of NFAT was determined with confocal microscopy. *F*, quantification of nuclear predominant fluorescence of GFP-NFAT4. *G*, effects of TRPC6 WT, C6-ΔN, and C6-3A on the ET-1-induced increase in NFAT-luciferase activity. Twenty-four h after infection, cells were treated with ET-1 for 48 h. *, $p < 0.05$ *versus* nontreatment (no ET-1) of control or LacZ-expressing cells. #, $p < 0.05$ *versus* ET-1 treatment of control or LacZ-expressing cells.

ionomycin-induced Ca^{2+} release were not affected by ET-1 treatment or TRPC6 siRNA treatment, the changes in TRPC6 proteins may not influence Ca^{2+} content of intracellular Ca^{2+} stores or IP_3-mediated functions.

Requirement of TRPC6 for ET-1-induced NFAT Activation—Since CA $G\alpha_{13}$-induced TRPC6 up-regulation enhances basal Ca^{2+} influx activity, we examined whether ET-1 treatment enhances basal Ca^{2+} influx activity through $G\alpha_{12/13}$-mediated TRPC6 up-regulation. Treatment with ET-1 for 48 h enhanced the increase in $[Ca^{2+}]_i$ induced by the addition of 2 mM Ca^{2+} to ET-1-containing Ca^{2+}-free solution, which was completely suppressed by TRPC6 siRNA (C6-1609) and DN TRPC6 (C6-ΔN) (Fig. 5, *A* and *B*). The ET-1-induced enhancement of Ca^{2+} influx was suppressed by p115-RGS and PP2. Treatment with ET-1 increased Src activity, which was completely suppressed by p115-RGS and PP2 but not by SP600125 (Fig. 5*C*). We confirmed that ET-1-induced TRPC6 up-regulation was not affected by PP2 (supplemental Fig. 2*C*). Src activation by ET-1 stimulation was mediated by ET_A receptor, since ET_A receptor-selective (BQ123) but not ET_B receptor-selective (BQ788) blockers inhibited ET-1-stimulated Src activation (supplemental Fig. 2*D*). These results suggest that $G\alpha_{12/13}$-mediated activation of Src tyrosine kinase participate in ET-1-induced increase in basal Ca^{2+} influx activity apart from TRPC6 up-regulation. On the other hand, treatment with ET-1 for 48 h induced nuclear localization of GFP-NFAT4 proteins, which were inhibited by p115-RGS and SP600125 (Fig. 5, *D* and *F*). Treatment with SP600125 (1 μM) significantly inhibited the ET-1 treatment-induced increase in basal Ca^{2+} influx activity (ΔRatio = 0.70 ± 0.05, n = 67 cells) and TRPC6 protein levels (Fig. 3*D*), suggesting that $G\alpha_{12/13}$-mediated activation of JNK participates in ET-1-induced NFAT translocation through TRPC6 up-regulation. The ET-1 treatment-induced NFAT translocation was also suppressed by TRPC6 siRNAs (Fig. 5, *E* and *F*). The expression of WT TRPC6 increased basal NFAT activity 2.5-fold, and it also enhanced NFAT activity induced by ET-1 treatment (Fig. 5*G*). In contrast, the expression of DN TRPC6 mutants completely suppressed the ET-1 treatment-induced increase in NFAT activity. These results suggest that $G\alpha_{12/13}$-mediated up-regulation and activation of TRPC6 channels participate in sustained activation of NFAT induced by ET-1 treatment in cardiac fibroblasts.

Inhibition of Cardiac Myofibroblast Formation by TRPC6 Activation—Transformation of cardiac fibroblasts to myofibroblasts is characterized by expression of α-SMA and production of ECM components that are a key event in connective tissue remodeling (6). Since NFAT is activated by the sustained increase in $[Ca^{2+}]_i$ and the calcineurin-NFAT